LBL-13227

Lawrence Berkeley Laboratory
UNIVERSITY OF CALIFORNIA

Materials & Molecular Research Division

THE DIFFUSION OF GASES IN CAPILLARIES

Nathan S. Jacobson
(Ph.D. thesis)

August 1981

TWO-WEEK LOAN COPY

This is a Library Circulating Copy which may be borrowed for two weeks. For a personal retention copy, call Tech. Info. Division, Ext. 6782

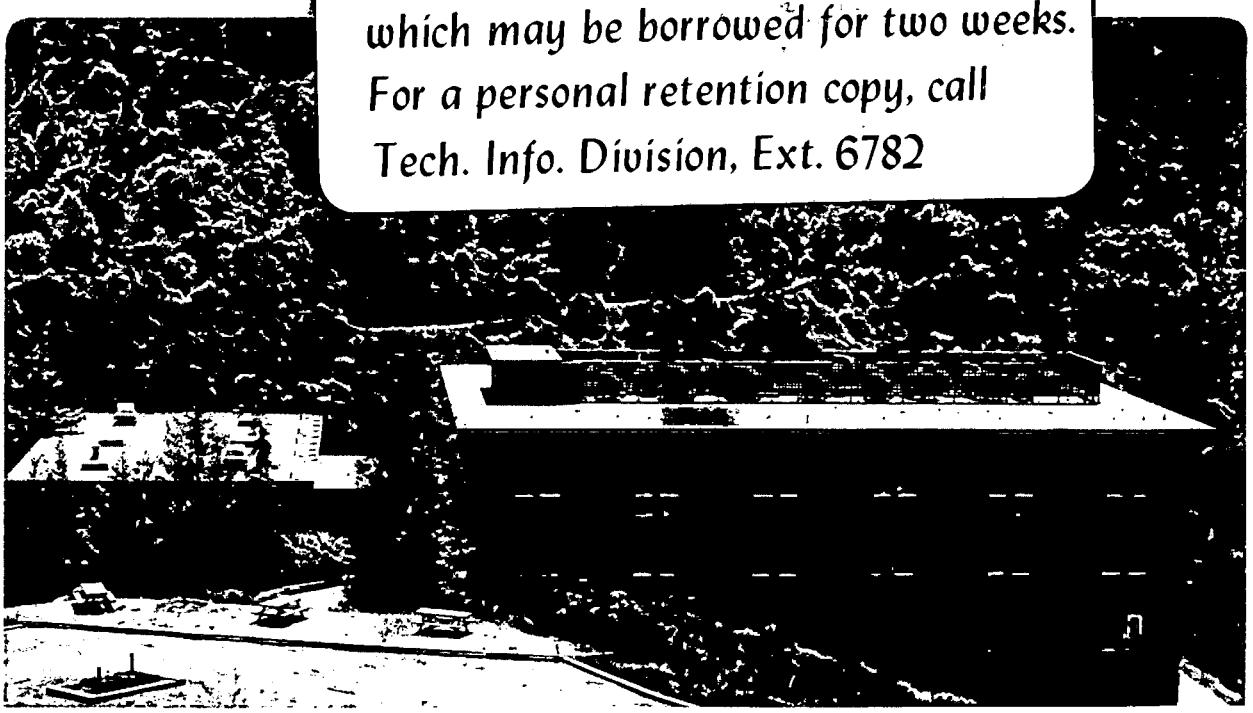

Prepared for the U.S. Department of Energy under Contract W-7405-ENG-48

DISCLAIMER

This document was prepared as an account of work sponsored by the United States Government. While this document is believed to contain correct information, neither the United States Government nor any agency thereof, nor the Regents of the University of California, nor any of their employees, makes any warranty, express or implied, or assumes any legal responsibility for the accuracy, completeness, or usefulness of any information, apparatus, product, or process disclosed, or represents that its use would not infringe privately owned rights. Reference herein to any specific commercial product, process, or service by its trade name, trademark, manufacturer, or otherwise, does not necessarily constitute or imply its endorsement, recommendation, or favoring by the United States Government or any agency thereof, or the Regents of the University of California. The views and opinions of authors expressed herein do not necessarily state or reflect those of the United States Government or any agency thereof or the Regents of the University of California.

THE DIFFUSION OF GASES IN CAPILLARIES

Nathan S. Jacobson

Materials and Molecular Research Division, Lawrence Berkeley Laboratory
and Department of Materials Science and Mineral Engineering
University of California, Berkeley, California 94720

ABSTRACT

Two aspects of the diffusion of gases in capillaries are explored. In Part I a Monte Carlo computer simulation of Knudsen flow is adapted to count collisions and record collision distributions. Using this simulation, the behavior of gases in both open and closed end tubes is examined. Given a tube with one end closed and a length-to-radius ratio of L/R, it is shown that a molecule that enters this tube will strike the wall an average of 2 L/R times before escaping. It is also shown that most molecules do not travel very far into the pore. However, those that reach the pore bottom usually strike the walls many times before escaping.

The average number of collisions a molecule undergoes in passing through an open-end capillary is also calculated. This has applications to reactive flow and heterogeneous catalysis. By knowing the average number of times a reactant molecule strikes the walls of a catalyst lined capillary, one can calculate a reaction probability. Two experiments based on this principle are proposed.

This work was supported by the Director, Office of Energy Research, Office of Basic Energy Sciences, Materials Science Division of the U.S. Department of Energy under Contract No. W-7405-ENG-48.

This manuscript was printed from originals provided by the author.

If the reaction probability is already known, the processes in a supported catalyst can be simulated. From this analysis the distribution of active material, pore size, and pellet diameter can be optimized for a given reaction. This approach may offer advantages over analytic models of diffusion and reaction in supported catalysts.

Part II is an experimental study of Knudsen and surface diffusion in porous alumina. This material had pores 1.1 π 1.3μ in diameter and was used as barriers 1.124 π .114 mm thick. It is shown that He, Ar, N_2, O_2, CO_2, CH_4, NH_3, and SO_2 all pass through these barriers by Knudsen diffusion at room temperature. At 631°K, zinc vapor also passes through this material by Knudsen flow. However, NaCl, NaF, and LiF vapors show substantial elements of surface diffusion with surface flux to Knudsen flux ratios of 1.6, 5.1, and 11.2, respectively. Apparently this is the first clear demonstration of the surface diffusion of high temperature vapors in porous media. Temperature dependence and Auger data indicate that the surface component is very likely a dilute two-dimensional gas. The use of high temperature vapors in conjunction with porous barriers appears to be a promising technique for studying surface-vapor interactions.

CONTENTS

Abstract i

GENERAL INTRODUCTION 1

PART I: WALL COLLISIONS IN KNUDSEN FLOW 4

1. Introduction 4
2. Calculation Method 6
3. Results and Discussion 6
4. Conclusion 19
Appendices I, II, III 21
References 40
Tables 42
Figure Captions 46
Figures 1-12 47

PART II: SURFACE DIFFUSION IN POROUS ALUMINA 59

1. Introduction 59
2. Characterization of Porous Alumina 67
3. Experimental 70
4. Results and Discussion 77
5. Conclusion 85
References 87
Tables 90
Figure Captions 92
Figures 13-23 93

ACKNOWLEDGMENT 104

GENERAL INTRODUCTION

The diffusion or flow of gases through capillaries is important in a number of areas. Among these are the transport of gas to the active sites in a supported catalyst, the escape of gas through the porous oxide in a decomposition reaction, and the transport of oxygen through soils to plant roots. This wide applicability is evident from the large body of literature on the subject.

Flow can be divided into two major regimes, depending on the relationship between λ, mean free path, and d, capillary diameter.[1] When $\lambda/d > \sim 10$, this is the Knudsen or molecular flow regime. Because the mean free path is so much greater than the pore diameter, molecule-molecule collisions are rare and molecule-wall collisions predominate. When $\lambda/d < \sim 0.01$, this is the hydrodynamic or viscous flow regime. Here molecule-molecule collisions are important and the gas flows as a fluid. Between the two, when $10 \geq \lambda/d \geq 0.01$, there is a transition region. The various flow regimes related to pore diameter, mean-free path, and hence pressure, are shown graphically in Fig. 1.

In the Knudsen flow regime, most molecules travel in straight lines until they encounter a surface. They momentarily adsorb on the surface and then leave the surface in a random direction that is independent of the incident direction. There is a finite probability that a molecule which has entered a channel will never reach the end, but rather reemerge from the entrance. Thus, Knudsen flow through channels can be characterized by a transmission probability, W:

$$W = \frac{\text{Number of molecules exiting}}{\text{Number of molecules entering}} = \frac{J_{out}}{J_{in}}$$

Knudsen first described this type of flow mathematically in 1909[2] and hence it bears his name. However, it was Clausing who first reported accurately calculated transmission probabilities.[3] Hence, transmission probabilities for Knudsen flow are freuqently referred to as "Clausing factors." For a straight cylindrical capillary, they are a function of the length-to-radius ratio only.

In 1960, Davis used a Monte Carlo method to model Knudsen flow.[4] Knudsen flow is well-suited to this type of model, because Knudsen flow is a random walk process in which each molecule acts independently of the others. Thus, the history of a single molecule can be traced until it is complete, and then the history of the next molecule can be traced. Davis obtains transmission probabilities equal to those calculated analytically by Clausing. This result is a good check of Davis's program.

In this thesis, two aspects of the behavior of vapors in the Knudsen flow regime are explored. In Part I, a computer program similar to that of Davis's is constructed. However, from the new program, the number of collisions a molecule undergoes in passing through a capillary is calculated. Collision numbers and collision densities along the capillary wall are important parameters, which yield interesting information about the behavior of gases in capillaries. In addition,

when these parameters are used in conjunction with a reaction probability, they have applications to heterogeneous catalysis.

Part II of this thesis is an experimental study of enhanced flow rates due to surface diffusion. Previous efforts to demonstrate a significant contribution of surface diffusion to flow of high temperature vapors through capillaries and orifices have not been conclusive. The present study, which employs porous barriers, yields conclusive evidence for surface diffusion and also yields some information on the mechanism of the process.

PART I: WALL COLLISIONS IN KNUDSEN FLOW

1. Introduction

Since the initial work of Davis in 1960, a number of investigators have used the Monte Carlo method to model Knudsen flow. Most notably, Ward et al. have modeled a large number of effects which occur in a Knudsen effusion cell. Among the parameters that they considered are the position of the sample, shape of the orifice, geometry of the cell, surface diffusion, and specular reflection.[5-11] Their results are typically presented in terms of angular distributions of molecules emerging from the orifice. Sandry and Stevenson have used the Monte Carlo simulation to examine molecules leaving curved surfaces inside cylindrical capillaries.[12]

One important parameter that is easily available from these simulations is the average number of collisions a molecule undergoes in passing through a capillary. Yet no one had reported these collision numbers. The closest that other investigators have come is to calculate the collision density along the walls of a capillary. From his early analytic calculations, Clausing[13] showed that this density drops off as 1/x where x is the distance along the tube. For a tube of length L and radius R, he found that the collision density between x and x + dx is given by:

$$g(x) = \alpha + (1 - 2\alpha)(L - x)/x$$

$$\alpha = \frac{\sqrt{L^2 + 4R^2} - L}{2R + \dfrac{4R^2}{\sqrt{L^2 + 4R^2}}}$$

In addition, Ward and Fraser[9] give some of their results in terms of collision densities.

The average number of collisions a molecule undergoes in passing through a capillary elucidates the behavior of molecules in capillaries and also has direct applications to heterogeneous catalysis. One of the most fundamental parameters in heterogeneous catalysis is the reaction probability, RP[14]:

$$RP = \frac{\text{Rate of formation of product molecules}}{\text{Rate of incidence of reactant molecules}}$$

$$= \frac{\text{Number of reactive collisions}}{\text{Total number of collisions}}$$

Reaction probabilities are a function of the particular reaction, the particular solid surface, the pressure, and the temperature. Values range from 10^{-1} to 10^{-11}. Somorjai[14] lists reaction probabilities for a number of organic reactions. Most industrial catalysts are inert porous materials with the active material on the pore walls. These pores can be approximated as straight capillaries. Knowing the number of collisions that unreacted molecules undergo before they reach a detector allows one to calculate a reaction probability. Conversely, if a reaction probability is already known, one can simulate diffusion and reaction in these porous catalyst pellets.

2. Calculation Method

Three main computer programs were used. The basic program for Knudsen flow was reconstructed from the article by Davis.[4] Appendix I gives a detailed description of this program and a listing of it.

The program by Davis was modified in several ways. The first modification was simply to count collisions. This procedure is also described in Appendix I. A second modification was to calculate the collision distribution along the capillary wall. However, most of the emphasis was on reactive collision calculations. For these a closed-end pore was used. Appendix II gives a description of this modification and a listing of the program.

The third program is an approximation. In order to model real catalytic systems, it was necessary to examine very long tubes. The computer time necessary to do so was excessive. Therefore, an approximation was developed: The capillary was treated as being composed of ten segments. The average behavior of a molecule in each segment is known. This program is described in detail in Appendix III.

3. Results and Discussion

Collision numbers: The first systems examined were open-end capillaries with length-to-radius ratios varying from 0.01 to 10,000. For 48 capillaries in this range, 100,000 molecules were followed from their entrance into the capillary to either their subsequent return to the entrance or their escape from the exit. Each time a molecule struck the capillary wall, a collision was counted. For length-to-radius ratios

from 0.01 to 100, the exact calculation was used. Beyond 100, the segment approximation was used. Table 1 lists the following quantities:

1) The average number of collisions for a molecule that returns to the capillary entrance,

2) The average number of collisions for a molecule that escapes from the capillary exit,

3) The average number of collisions per molecular journey--i.e., both returns and escapes.

Note that the difference between quantities 1 and 2 grows rapidly with increasing length-to-radius ratio. For very long capillaries, molecules that escape strike the wall many more times than those that return. Note also that the average number of collisions per molecular journey is quite close to the length-to-radius ratio. This remarkable result holds over six orders of magnitude. These collision numbers can be applied to heterogeneous catalysis, as will be discussed in the next section.

The collision density along the capillary walls can be obtained by dividing the capillary into segments and recording the number of collisions in each segment. For an open-end pore, a linear gradient is obtained. This is shown graphically in Fig. 2 for a capillary with a length-to-radius ratio of 100, divided into 10 segments. As mentioned in the introduction, Clausing derived a collision density from the analytic formulation of Knudsen flow. In order to apply his equation to a segment of finite length, the equation must be integrated from one end of the segment to the other:

$$s = \int_{x_1}^{x_2} g(x)\, dx = (1-\alpha)(x_2 - x_1) - (1-2\alpha)\,(x_2^2 - x_1^2)/2L$$

$$\alpha = \frac{\sqrt{L^2 + 4R^2} - L}{2R + \dfrac{4R^2}{\sqrt{L^2 + 4R^2}}}$$

x_1 and x_2 are the beginning and end of the segment, and L and R are the length and radius. To compare to the Monte Carlo calculation, s is normalized to the number of collisions. Normalization is done by means of a one variable least-squares calculation: S = as where $a = \Sigma\, s_i t_i / \Sigma\, s_i^2$. t_i's are the Monte Carlo results. A comparison of Monte Carlo results with analytic results is shown in Table 2. The results are similar, as they should be.

Capillaries with one end closed were also considered using the Monte Carlo method. Five capillaries with length-to-radius ratios varying from 1 to 200 were examined. The average number of wall collisions per molecular journey, i.e., from entrance of the molecule into the capillary to its subsequent reemergence, was calculated. Table 3 shows that this quantity is close to twice the length-to-radius ratio for a closed-end capillary. This result was expected on the basis of the open-end capillary results.

The collision density along the walls of a closed-end capillary was calculated. Figure 3 gives this result for a length-to-radius ratio of 100 and a sample size of about 50,000. The results could have been

predicted--a constant pressure throughout the capillary. The Monte Carlo method allows one to further isolate the behavior of the individual molecules. Figure 4 is a plot of number of molecules vs maximum depth of travel. Clearly, most of the molecules do not go very far into the pore. The question then is where do most of the collisions near the pore bottom come from.

Apparently those molecules that do reach the bottom of the pore undergo many collisions before escaping. This assertion can be checked by counting the number of collisions with the pore bottom. Table 3 gives this number for closed-end capillaries varying from 1 to 200 and a sample size of 100,000 molecules. In each case, the number of collisions with the capillary bottom is close to 100,000. Thus, although only a fraction W (the transmission probability) of the molecules that enter the capillary reach the bottom, each molecule in this fraction strikes the bottom an average of 1/W times.

This result corroborates the analytic calculations of Meschi and Searcy.[15] They define f_n as the fraction of molecules leaving the pore entrance after n visits to the pore bottom:

$$f_o = 1 - W$$
$$f_1 = W^2$$
$$f_2 = W^2 (1-W)$$
$$\vdots$$
$$f_n = W^2 (1-W)^n$$

W is the transmission probability for an open-end pore with the same length-to-radius ratio. The sum of f_n from zero to infinity is equal

to one, as it should be. The important parameter is $\bar{n}$, the mean number of collisions with the pore bottom:

$$\bar{n} = \sum_{n=0}^{\infty} n\, f_n = \sum_{n=1}^{\infty} n\, W_2(1-W)^{n-1} = 1$$

Thus, regardless of pore depth, the mean number of collisions with the pore bottom equals one. This means that although only a fraction W actually reach the bottom of the pore, each molecule in this fraction will strike the pore bottom an average of 1/W times. This, of course, is the result reached by the Monte Carlo method.

These results have lea to a number of interesting conclusions about the behavior of gases in both open- and closed-end capillaries. Applications to the flow of reactive gases and heterogeneous catalysis are discussed below.

Applications to reactive gases: By knowing the average number of collisions a reactant molecule undergoes before it or its reaction product reaches a detector, one can calculate a reaction probability. Consider the first-order reaction $A \rightarrow bB + cC$ under conditions such that product formation is so much thermodynamically favored that the back reaction can be neglected. However, there is a kinetic barrier to the prooucion of B and C. The probability that molecule A will react upon striking a catalytic surface is RP. The probability that it will not react is (1-RP). When one considers multiple collisions, it is easier to evaluate (1-RP) as a function of the number of collisions. This

procedure avoids the problem of a reacted molecule undergoing additional surface collisions. Suppose the reactant molecules undergo m collisions before they reach a detector. Then $(1-RP)^m = x$, where x is the fraction of A molecules at the detector. Solving for RP gives $RP = 1 - x^{1/m}$.

A typical reaction probability for a hydrocarbon conversion is 10^{-6}. To obtain a 50 percent conversion requires approximately 10^6 collisions.

Based on this principle, two experimental approaches for determining reaction probabilities are proposed. They are illustrated in Fig. 5. Figure 5a shows a stream of gas A flowing past a porous plug with a catalytically active material uniformly distributed in the pores. The stream can be in the hydrodynamic flow regime. However, the flow through the porous plug to the detector must be in the Knudsen flow regime. In order to obtain 10^6 collisions, capillaries with a length-to-radius ratio of approximately 1000 (cf., Table 1) must be used. Machining these is not really practical, so a porous plug is used. The porous plug has tortuous channels, so the collision number used is only an estimate of the actual number of collisions. Note that the collision number used is only for molecules that escape; those that return are swept away in the flowing stream.

This method has the problem that there is a concentration gradient of both reactant and product through the porous plug. Reaction probabilities may be sensitive to these concentrations, and therefore the

measured reaction probability may be a function of the particular pressure gradient established by the barrier.

However, this particular catalyst arrangement could be of value in a reaction such as $A_2 \rightarrow 2A$. The pressure gradient would tend to push the equilibrium to the products. Thus, the pressure gradient may make it possible to carry out the reaction at a lower temperature.

Figure 5B shows a second arrangement for measuring reaction probabilities. This is a chamber with a source of gas A, a pumping port, a supported catalyst, and an orifice to a detector. A supported catalyst is a highly porous pellet with the active material deposited on the interior. Such a catalyst can be modeled as a series of dead end pores with length equal to the pellet's radius. The average number of collisions in a dead end pore is known to be approximately 2L/R (cf., Table 3). So the average number of collisions a molecule undergoes inside a pellet before leaving the orifice is:

$$m = \frac{A(\text{external-catalyst pellet}) \times \varepsilon \times 2L/R \times f}{A(\text{orifice}) + A(\text{pumping port})}$$

Here A is an area, ε is the fractional area fronted by pores, and f is the fraction of pore surface occupied by the uniformly distributed catalyst. The purpose of the pumping port is to avoid accumulation of product in the chamber. The port acts like a second orifice and therefore must be included in the denominator. Putting the above expression for m into $RP = 1 - x^{1/m}$ gives the reaction probability.

Past measurements of reaction probabilities usually use a flow system and a low surface area catalyst, such as a wire, foil, or pellet with large pores.[16-18] The downstream gas is analyzed and the reaction rate per unit area of catalyst is determined. With this information and the flux striking the catalyst, the reaction probability can be calculated. The two methods proposed here apply to high surface area supported catalysts, which may be like those used industrially.

Thus, by knowing the average number of collisions a reactant molecule undergoes with a catalytic surface, one can calculate a reaction probability. Conversely, if the reaction probability is already known, one can design a catalyst with the requisite number of collisions.

As mentioned, many industrial catalysts are supported metal catalysts. For these, the pores of an inert porous material are impregnated with catalytically active particles 1-10 nm in diameter. For many applications, this active material is platinum or palladium. A supported catalyst gives the desired high surface area with a minimal use of precious metal.

When catalysts are used in porous supports, the active material near the outside of the pellet is much more accessible to the reactant than is the active material near the pellet's interior. If the reaction probability is high, the active material at the end of a long pore may seldom be reached by an unreacted molecule. It is therefore important to determine what pellet size and what distribution of active material will efficiently utilize the precious metal. This problem was first addressed by Thiele.[19] Since then, many other investigators have studied

it.[20] In a typical analysis, diffusion equations are coupled with reaction rate equations. An even distribution of active material throughout the pellet is assumed and the back reaction is assumed to be negligible. The results are usually reported as a plot of effectiveness factor, η, vs Thiele modulus, ϕ. The effectiveness factor is the ratio of the actual reaction rate to the rate that would occur if there were no diffusion limitations. The Thiele modulus is also a dimensionless quantity. For a spherical pellet, it is $\phi = R/3 \sqrt{K_v c_s^{m-1}/D_{eff}}$, where R is the radius of the sphere, K_v is the rate constant, c_s is the reactant concentration at the outside of the pellet, m is the order of the reaction, and D_{eff} is the effective diffusion coefficient.

Clearly, an effectiveness factor of one is most desirable. This condition is approached for small values of ϕ. Hence, small pellet size and large diffusion coefficients will minimize diffusion limitations. Note also that, since the catalyst is evenly distributed throughout the pellet, catalysts with smaller rate constants have better effectiveness factors than catalysts with high rate constants. Thus, active catalysts such as platinum and palladium generally have low effectiveness factors. This means larger diffusion limitations. Hence, these materials are often placed on the outer edges of the support.

The distribution of active material in a pellet can be accurately controlled.[21,22] Although noble metal reforming catalysts generally have the active material at the outer edges, Wei and Becker show that for carbon monoxide oxidation the catalyst is more effective if placed at the

center of the pellet.[23] They believe this is due to the negative order reaction rate dependence on carbon monoxide concentration. Catalyst poisoning may also make an interior distribution more desirable. These observations and applications of effectiveness factors give qualitative data on the preferred location of the active material, but yield nothing quantitative.

By looking at reaction probabilities in conjunction with the Monte Carlo simulation, one can make some quantitative predictions. In a supported catalyst under Knudsen flow conditions, a reactant molecule diffuses in, moves around at random until it reacts or escapes, and finally the product escapes. Here the pores are modeled as straight capillaries with one end closed. A molecule is allowed to diffuse into a pore and given a probability of reacting. The molecule's journey is traced until it escapes, and then another molecule is examined. This program is described in detail in Appendix II. The final results are a plot of the number of reactive collisions as a function of pore depth. Figure 6 shows the distribution of reactive collisions for a closed-end capillary with a length-to-radius ratio of 100, a reaction probability of 10^{-2}, and a sample size of 100,000 molecules. For this short pore, most of the reactive collisions occur within the first 40 percent of pore depth.

Real catalysts, which operate in the Knudsen flow regime, typically have very small pores. Figure 1 shows that, in order to obtain Knudsen flow at near atmospheric pressure, the pores must be in the 10 nm range. Also, typical reaction probabilities for hydrocarbon conversions

are 10^{-6} or less. Consider the high surface catalyst discussed by Nutall,[21] which he identifies as 3449-11A UOP alumina pellet:

Support diameter--.32 cm

Modal pore radius--1.7×10^{-6} cm

Surface area--149 m^2/gr.

This means that if one models the pellet as a dead end pore, its length-to-radius ratio is approximately 10^5. As indicated, most collisions occur at the mouth of the pore, so the precise pore length is not important. Modeling this long pore exactly requires an inordinate amount of computing time. So the segment approximation described in Appendix III was used. Initially, the capillary was divided into ten segments and the number of reactive collisions in each segment was counted. However, for reaction probabilities greater than 10^{-7}, most of the reactive collisions occurred in the first segment. Therefore, this segment was divided into ten smaller segments. It should be noted that dividing the pore into smaller segments gives a more accurate result for the total number of reactive collisions. This is an expected consequence of the segment approximation.

Three reactions, representing a range of reaction probabilities, were selected from the literature. The catalytic material for each reaction is polycrystalline platinum. In each case, the pore has a length-to-radius ratio of 10^5, a sample size of one million molecules was used, and the fraction of reactive collisions was plotted as a function of distance into the pore. The results are given in Figs. 7, 8, and 9.

Figure 7 gives the results for ammonia decomposition:

$$2\ NH_3 \rightarrow N_2 + 3\ H_2$$

The reaction probability is 3.3×10^{-3} at T = 1200°K and an ammonia pressure between 1.3×10^{-5} and 2.6×10^{-2} atm.[24] The results for this relatively high reaction probability indicate all the reactive collisions occur in the first one percent of the pore. Thus, platinum need only be placed in a narrow band around the support.

Figure 8 gives the results for ethylene hydrogenation:

$$H_2C = CH_2 + H_2 \rightarrow H_3C - CH_3$$

The reaction probability is 6.3×10^{-7} at T = 273°K and a partial pressure of ethylene and hydrogen of about .1 atm each.[25] The results for this intermediate reaction probability indicate the reactive collisions extend several percent into the pore. Thus, platinum should be dispersed a little further into the support.

Figure 9 gives the results for propane hydrogenolysis:

$$H_3C - CH_2 - CH_3 + H_2 \rightarrow H_3C - CH_3 + CH_4$$

The reaction probability is 5×10^{-9} at T = 633°K and a propane partial pressure of about .01 atm and a hydrogen partial pressure of about .1 atm. The results for this relatively low reaction probability indicate the reactive collisions extend about 40 percent into the pore. Thus, platinum should be dispersed well into the support.

Unfortunately, there is very little experimental data with which to compare these predictions. The generalization that platinum reforming catalysts need only a band of platinum along the edge of the support would not be true for reactions with very low reaction probabilities. For carbon monoxide oxidation, the better performance of the interior deposit can probably be explained by a low reaction probability, as well as the negative order dependence on carbon monoxide concentration.

It is important to note that extending a pore beyond the length at which reactive collisions become negligible does not alter the results. Thus, these calculations can be used to predict pellet and pore sizes. For the high probability reactions, pellets with pores that have length-to-radius ratios of about 10^3 could be used. Even for the low probability reaction (Fig. 9), it is evident that ~95 percent of the reaction occurs in the first 50 percent of the pore length. Thus, pellets with pores that have length-to-radius ratios of about 5×10^4 could be used. If pellets of one-half the assumed pellet diameter, but unchanged pore diameter, were used, essentially the same reaction rate could be obtained with a reactor volume one-eighth of that required by the original pellets.

Of course, a real supported catalyst differs from this approximation in several important ways: (a) the pores are tortuous--multiply bent, cross-linked, and of varying cross-sectional area; (b) the active material is not uniformly distributed along the pore walls, but rather in small granules dispersed along the pore; (c) the concentration profile of both the reactants and the products changes

throughout the support, which may result in a differing reaction probability; and (d) the molecule may emerge from the pore and reenter another pore.

Nevertheless, this simulation does approximate the behavior of a supported catalyst. It can be regarded as a first step toward a complete model. Evans et al.[27] have simulated Knudsen flow in porous media. As more detailed information becomes available for kinetics on surfaces, it should be possible to compensate for (c). Thus, a detailed simulation of the processes in a supported catalyst could develop. Because it is a simulation, it offers advantages over traditional models of diffusion and reaction in predicting optimum conditions in a porous catalyst pellet.

4. Conclusions

Collision numbers have been extracted from the Monte Carlo simulation of Knudsen flow. This important parameter leads to a number of interesting results. Forty-eight capillaries with length-to-radius ratios varying from 0.01 to 10,000 were examined. For each capillary the average number of collisions per return, average number of collisions per escape, and average number of collisions per molecular journey are tabulated. These numbers find applications to heterogeneous catalysis. Collision densities along the capillary walls are also calculated. These indicate a linear pressure gradient, as predicted by the analytic treatment of Knudsen flow.

For a closed end pore, the average number of collisions per molecular journey is approximately twice the length-to-radius ratio.

Such a pore has a constant pressure throughout. Most of the molecules really do not go very far into the pore. However, those that do typically then strike the wall many times before escaping.

These calculations have application to reactive flow and heterogeneous catalysis. Two experiments for measuring reaction probabilities on catalytic surfaces are proposed. They are based on a knowledge of the average number of times a reactant molecule strikes the catalytic surface before reaching a detector.

If the reaction probability is already known, diffusion and reaction can be simulated in a supported catalyst. This approach may offer advantages over traditional analytic models of diffusion and reaction. The catalyst is modeled as a straight, closed end pore with a uniform distribution of active material. This model gives the number of reactive collisions as a function of depth into the pore. The results can be used to design catalyst supports of optimum pore geometry for a given reaction and catalyst.

Appendix I. The Monte Carlo Simulation

A program similar to that of Davis[4] was used. Here his equations are carefully re-derived and explained. Some simplifications and additions are also discussed.

First, a cylinder is defined with radius one and length L. The length and all other distances are measured in terms of radii units. A coordinate system is defined with the z axis along the length of the cylinder and the x and y axes at the base. The origin is at the bottom center of the cylinder.

Now a molecule diffuses into the cylinder. It is given a random starting point at the base of the cylinder as follows:

$$x = 2R_1 - 1 \qquad -1 < x < 1$$

$$y = 2R_2 - 1 \qquad -1 < y < 1$$

where R_1 and R_2 are random numbers between zero and one. If the point lies outside the base, another point is selected.

Next, the molecule is given a direction. Molecules must leave the starting point with a cosine distribution per unit solid angle. The direction of the molecule is given in terms of the spherical coordinates θ and ϕ. θ varies between 0 and $\pi/2$ and follows a special distribution, which will be discussed. ϕ varies between 0 and 2π and is completely random.

Figure 10a shows a molecule from a point P traveling along a line to an element of solid angle, $d\omega$. For a cosine distribution, the fraction of molecules traveling along this line is proportional to $\cos\theta$ and $d\omega$. Thus, $dN \alpha \cos\theta \, d\omega$. Consider the hemisphere around point P to

clarify $d\omega$. This is an element of solid angle, equal to $\sin\theta\, d\theta\, d\phi$. Since only θ has been specified, ϕ varies from 0 to 2π. Thus, $d\omega = 2\pi \sin\theta\, d\theta$ and $d\omega$ is an infinitesimal band in the hemisphere, as shown in Fig. 10b. This means $dN\alpha \cos\theta\, d\omega = 2\pi \sin\theta \cos\theta\, d\theta$. The angle θ follows a sine-cosine distribution.

The next step is to generate this distribution on the computer. Nearly every computer has a built-in routine which generates random numbers between 0 and 1 in an equiprobable distribution. The problem is to go from an equiprobable distribution to a sine-cosine distribution. There are several ways to do this. The method of Davis is to generate two random numbers R_1 and R_2 and take the larger of the two. This gives the probability distribution $P(R)dR = 2\, RdR$. That is, the larger R is, the more chance of choosing it. Let $R = \cos\theta$:

$$P(R)dR = P(\cos\theta)\, dR/d\theta\, d\theta = 2 \cos\theta \sin\theta\, d\theta$$

This gives the desired cosine-sine distribution. An alternate method is given by Hamming.[28] He describes a method to go from an equiprobable distribution to another distribution. Using his method to obtain a cosine-sine distribution for θ, gives $\theta = \arcsin \sqrt{R}$, where R is a random number between 0 and 1.

As mentioned previously, ϕ is chosen randomly between 0 and 2π. The actual program requires sines and cosines of ϕ. These can be generated from $\sin(2\pi R)$ and $\cos(2\pi R)$, where R is a random number between 0 and 1. However, trigonometric functions are calculated by a series in

the computer, and for a large number of calculations this procedure may require considerable computer time. Von Neumann[29] describes a method to avoid this. He takes a rectangle formed by the random numbers u and v, which varies between 0 and 1:

$$\sin \delta = \pm u/(u^2+v^2)^{1/2} \qquad \cos \delta = \pm v/(u^2+v^2)^{1/2}$$

The square root can be avoided by using the half-angle formula $\cos \phi = \cos 2\delta = 1 - (2 \sin^2 \delta)$. For ϕ to vary between 0 and 2π, δ must vary between 0 and π. This is done by taking a rectangle with the sides:

$$u = 2 R_1 - 1 \qquad 0 < R_1 < 1 \qquad -1 < u < 1$$

$$v = R_2 \qquad 0 < R_2 < 1 \qquad 0 < v < 1$$

$$\cos \phi = \cos 2 \delta = 1 - \frac{2 v^2}{(u^2 + v^2)} = \frac{(2R_1 - 1)^2 - R_2^2}{(2R_1 - 1)^2 + R_2^2}$$

$$\sin \phi = 2 \sin \delta \cos \delta = \frac{2(2R_1 - 1) R_2}{(2R_1 - 1)^2 + R_2^2}$$

Thus, sines and cosines of the random angle ϕ can be generated without using the more time-consuming functions.

Now θ and ϕ have been chosen appropriately. In order to simplify further calculations, the direction the molecule leaves the surface is given in terms of the direction cosines:

$$\cos \alpha = \sin\theta \sin \phi$$

$$\cos \beta = \sin \theta \cos \phi$$

$$\cos \gamma = \cos \theta$$

Note that $\cos^2\alpha + \cos^2\beta + \cos^2\gamma = 1$. Now the first flight of the molecule is traced. In order to determine what the molecule does--whether it strikes the wall or escapes--a distance criterion is used.

First, the distance from the base of the cylinder, along the specified direction to the wall, is calculated. This is shown as DW in Fig. 11a. From this figure:

$$(DW)^2 = h^2 + u^2 \qquad h^2 = (DW)^2 \cos^2\gamma$$

Now u is expressed in terms of α, β, x, and y. Consider the base of the cylinder in Fig. 11b. By the law of cosines:

$$u^2 = A^2 + B^2 - 2AB \cos \psi = 1+x^2+y^2 - 2\sqrt{x^2+y^2} \cos \psi$$

Cos ψ can be calculated from the dot product of A and B.

$$\vec{A} \cdot \vec{B} = AB \cos \psi$$

$$\cos \psi = \frac{\vec{A} \cdot \vec{B}}{AB} = \frac{(x,y)[x + (DW) \cos \alpha,\ y + (DW) \cos \beta]}{\sqrt{x^2 + y^2}}$$

$$= \frac{x^2 + (DW)\ x \cos \alpha + y^2 + (DW)\ y \cos \beta}{\sqrt{x^2 + y^2}}$$

So now u can be calculated:

$$u^2 = 1 + x^2 + y^2 - 2(x^2+y^2+(DW)\ x \cos \alpha + (DW)\ y \cos \beta)$$

$$u^2 = 1 - (x^2+y^2) - 2(DW)(x \cos \alpha + y \cos \beta)$$

The notation of Davis is used in order to simplify the expressions:

$$D = (x^2+y^2) - 1$$

$$Q = x \cos \alpha + y \cos \beta$$

$$P = \cos^2\alpha + \cos^2\beta \qquad 1-P = \cos^2\gamma$$

$$u^2 = -D - 2(DW)Q$$

$$(DW)^2 = h^2 + u^2 = (DW)^2(1-P) - D - 2(DW)\ Q$$

$$0 = P(DW)^2 + 2Q(DW) + D$$

Solving this quadratic gives DW in terms of the starting point (x,y) and the direction cosines (α,β):

$$DW = -Q/P \pm [Q^2/P^2 - D/P]^{1/2}$$

The next step is to calculate the distance along this direction to the top. This is given by $DT = L/\cos\gamma$. If the distance to the top is shorter than the distance to the wall, the molecule escapes from the top. The escape counter is increased by one and the program begins with a new molecule. If the distance to the wall is shorter than the distance to the top, the molecule strikes the wall and a wall collision is counted.

Once a wall collision has occurred, the coordinates of the collision points must be determined. The important one of these is $z(new) = z(old) + (DW)\cos\gamma$. Due to the symmetry of the system, x can be set to one and y can be set to zero. This facilitates further calculations. New direction cosines are selected--$\cos\alpha$, $\cos\beta$, and $\cos\gamma$. Now α must follow a sine-cosine distribution. Next, three distances are calculated along this line:

1) The distance from wall to wall. This is from the equation for DW derived earlier, but with x=1 and y=0:

$$DW = 2\cos\alpha/(1-\cos^2\gamma)$$

2) The distance from wall to bottom:

$$DB = -z/\cos\gamma$$

3) The distance from wall to top:

$$DT = L-Z/\cos\gamma$$

Either (2) or (3) will be negative, in which case it is set to a large positive number. As before, whichever distance is shortest determines the event. If there is a wall collision, the program counts one collision, generates three new direction cosines, and calculates three

new distances. If the molecule returns to the bottom, the program increments the return counter by one and begins again with a new molecule. If the molecule escapes from the top, the program increases the escape counter by one and begins again with a new molecule. After a specified number of molecules have been examined, the program stops and prints out the data.

The following is a listing of the program. It gives the average number of collisions for a molecule that escapes from the capillary and the average number of collisions for a molecule that returns. As a check, it also gives the Clausing factor, which is simply the number of escapes divided by the total number of molecules.

```
      PROGRAM RDN(INPUT, OUTPUT)
      L=100
      ESC=0.
      RET=0.
      COLL=0.
      CESC=0.
      CRET=0.
      I=0
      E=0.
      R=0.
C
    1 I=I+1
      IF (E .EQ. 1) CESC=CESC+COLL
      IF (R .EQ. 1) CRET=CRET+COLL
      E=0.
      R=0.
      COLL=0.
      IF (WARN(0) .NE. 0) GO TO 2
      IF (I .EQ. 100001) GO TO 2
C     CHOOSE RANDOM STARTING POINT
   21 X=2*RANF(N)-1
      Y=2*RANF(N)-1
      W=X**2+Y**2
      IF (W .GT. 1) GO TO 21
      Z=0
C
C     CHOOSE DIRECTION COSINES
C     GAMMA FOLLOWS A COSINE DISTRIBUTION
      CALL COSDIS(CGAM, CALP, CBET)
C
C     CALCULATE DISTANCE TO THE WALL
      D=(X**2+Y**2)-1
      Q=X*CALP+Y*CBET
      P=1-CGAM**2
      U=SQRT(Q**2-P*D)/P
      SW=-Q/P+U
C
C     CALCULATE DISTANCE TO THE TOP
      ST=L/CGAM
C
C     COMPARE SW TO ST
      IF (SW .LT. ST) GO TO 4
    3 ESC=ESC+1
      E=1.
      GO TO 1
C
C     WALL COLLISION
    4 Z=Z+SW*CGAM
      COLL=COLL+1
C
C     CHOOSE NEW DIRECTION COSINES
C     ALPHA FOLLOWS A COSINE DISTRIBUTION
      CALL COSDIS(CALP, CBET, CGAM)
C
C     CALCULATE WALL TO WALL DISTANCE
      SW=2*CALF/(1-CGAM**2)
C
C     CALCULATE WALL TO BOTTOM DISTANCE
      SB=-Z/CGAM
      IF (SB .LT. 0) SB=1.0E10
C
C     CALCULATE WALL TO TOP DISTANCE
```

```
      ST=(L-Z)/CGAM
      IF (ST .LT. 0) ST=1.0E10
C
C     COMPARE THE THREE DISTANCES
      IF (SW .GT. ST) GO TO 5
      IF (SW .GT. SB) GO TO 5
C     ANOTHER WALL COLLISION
      GO TO 4
    5 IF (ST .GT. SB) GO TO 7
      GO TO 3
    7 RET=RET+1
      R=1.
      GO TO 1
C
    2 PRINT 80, CESC, CRET, ESC, RET
   80 FORMAT (*1*, * CESC=*, F12.2, * CRET=*, F12.2, * ESC=*, F8.2,
     1* RET=*, F8.2)
      CLF=ESC/(I-1)
      ACESC=CESC/ESC
      ACRET=CRET/RET
      PRINT 85, L, CLF, ACESC, ACRET
   85 FORMAT (* FOR L/R = *, I3, * THE CLAUSING FACTOR IS *, F6.5, /,
     1 * AV. NO. COLLISIONS PER ESCAPE IS *, F12.4, /,
     2 * AV. NO. COLLISIONS PER RETURN IS *, F12.4)
      IF (WARN(0) .EQ. 0) GO TO 73
      PRINT 97
   97 FORMAT (/, * APPROACHING TIME LIMIT*)
      GO TO 74
   73 CONTINUE
   74 CONTINUE
      END
C
C
      SUBROUTINE COSDIS(CA, CB, CC)
C     GENERATES THREE DIRECTION COSINES
    1 U1=RANF(N)
      U2=RANF(N)
      DEN=(2*U1-1)**2+U2**2
      IF (DEN .GE. 1) GO TO 1
      CPH=((2*U1-1)**2-U2**2)/DEN
      SPH=2*(2*U1-1)*U2/DEN
    2 U3=RANF(N)
      U4=RANF(N)
      IF (U3 .LT. U4) GO TO 2
      CTH=U3
      STH=SQRT(1-CTH**2)
      CA=CTH
      CB=STH*CPH
      CC=STH*SPH
      END
```

777777777.777777777.777777777.777777777.777777777.777777777.777777777.777777777
777777777.777777777.777777777.777777777.777777777.777777777.777777777.777777777
777777777.777777777.777777777.777777777.777777777.777777777.777777777.777777777

Appendix II: Modification for Closed End Pores and Reactive Flow

The program described in Appendix I was modified to model reactive flow in a closed end tube. Instead of escaping from the end of the tube, the molecule strikes a disk at this end and returns back in the opposite direction. Due to the symmetry of the problem, the point of collision can be chosen randomly on the end disk of the tube.

To include the effects of reactive flow, a random number is generated on each collision. If the random number is less than the reaction probability, the molecule reacts. Otherwise, it does not. The tube is divided into 10 segments and the number of reactive collisions in each segment is tabulated.

A listing of the program follows.

```
      PROGRAM RDN(INPUT, OUTPUT)
C     CALCULATES REACTIVE COLLISION DISTRIBUTION FOR A CLOSED END PORE
C     J HOLDS SORTED Z COORDINATES OF COLLISIONS
      DIMENSION J(10)
      COMMON X, Y, CALP, CBET, CGAM
      READ 1, L
    1 FORMAT (I4)
      READ 7, PROB
    7 FORMAT (1F5.3)
      DO 10 K=1, 10
   10 J(K)=0
      COLL=0.
      TOP=0.
      I=0
C
   15 IF (WARN(0) .NE. 0) GO TO 45
      I=I+1
      IF (I .EQ. 100001) GO TO 45
      R=2.
C     CHOOSE RANDOM STARTING POINT
      CALL RSP(X,Y)
C
C     CHOOSE DIRECTION COSINES
C     GAMMA FOLLOWS A COS-SIN DISTRIBUTION
      CALL CSDIS(CGAM,CALP,CBET)
C
C     CALCULATE DISTANCE TO THE WALL
      CALL DTW(SW)
C
C     CALCULATE DISTANCE TO THE TOP
      ST=L/CGAM
C
C     COMPARE SW TO ST
      IF (SW .LT. ST) Z=SW*CGAM
      IF (SW .LT. ST) GO TO 25
C
C     COLLISION WITH TOP
   20 TOP=TOP+1
      IF (R .LE. PROB) GO TO 21
      R=RANF(N)
      IF (R .LE. PROB) J(10)=J(10)+1
   21 CONTINUE
C
C     CHOOSE COLLISION POINT AT RANDOM
      CALL RSP(X,Y)
C
C     CHOOSE DIRECTION COSINES
C     GAMMA FOLLOWS A COS-SIN DISTRIBUTION
      CALL CSDIS(CGAM,CALP,CBET)
C
C     CALCULATE DISTANCE TO THE WALL
      CALL DTW(SW)
C
C     CALCULATE DISTANCE TO THE BOTTOM
      SB=L/CGAM
C
C     COMPARE SW TO SB
      IF (SW .LT. SB) Z=L-SW*CGAM
      IF (SW .LT. SB) GO TO 25
      GO TO 15
C
C     WALL COLLISION
```

```
   25 COLL=COLL+1
      IF (R .LE. PROB) GO TO 26
      R=RANF(N)
      IF (R .GT. PROB) GO TO 26
      DO 30 N=1, 10
      Z1=FLOAT(L)*(N-1.)/10.
      Z2=FLOAT(L)*FLOAT(N)/10.
   30 IF (Z .GT. Z1 .AND. Z .LE. Z2) J(N)=J(N)+1
   26 CONTINUE
C
C     CHOOSE NEW DIRECTION COSINES
C     ALPHA FOLLOWS A COS-SIN DISTRIBUTION
      CALL CSDIS(CALP,CBET,CGAM)
C
C     CALCULATE WALL TO WALL DISTANCE
      SW=2*CALP/(1-CGAM**2)
C
C     CALCULATE WALL TO BOTTOM DISTANCE
      SB=-Z/CGAM
      IF (SB .LT. 0) SB=1.0E10
C
C     CALCULATE WALL TO TOP DISTANCE
      ST=(L-Z)/CGAM
      IF (ST .LT. 0) ST=1.0E10
C
C     COMPARE THE THREE DISTANCES
      IF (SW .GT. ST) GO TO 35
      IF (SW .GT. SB) GO TO 35
C     ANOTHER WALL COLLISION
      Z=Z+CGAM*SW
      GO TO 25
   35 IF (ST .GT. SB) GO TO 15
      GO TO 20
C
   45 II=I-1
      PRINT 2, II, COLL, TOP
   2  FORMAT (*1*, *II= *, I7, * COLL= *, F12.2, * TOP= *, F8.2)
      AVC=COLL/II
      PRINT 3, L, AVC
   3  FORMAT (* FOR L/R= *, I4, * AV. NO. COLLISIONS PER JOURNEY IS *,
     1F12.4)
      PRINT 100, PROB
  100 FORMAT (* PROB= *, F5.3)
      DO 50 M=1, 10
      PRINT 4, M, J(M)
   4  FORMAT (/, * FOR RING *, I3, * NO. OF REACTIVE COLLISIONS= *, I10)
   50 CONTINUE
      IF (WARN(0) .EQ. 0) GO TO 55
      PRINT 5
   5  FORMAT (/, * APPROACHING TIME LIMIT*)
   55 CONTINUE
      END
C
C
      SUBROUTINE RSP(X,Y)
   1  X=2*RANF(N)-1
      Y=2*RANF(N)-1
      W=X**2+Y**2
      IF (W .GT. 1) GO TO 1
      END
C
C
```

```
      SUBROUTINE DTW(SW)
      COMMON X, Y, CALP, CBET, CGAM
      D=(X**2+Y**2)-1
      Q=X*CALP+Y*CBET
      P=1-CGAM**2
      U=SQRT(Q**2-P*D)/P
      SW=-Q/P+U
      END
C
C
      SUBROUTINE CSDIS(CA, CB, CC)
C     GENERATES THREE DIRECTION COSINES
C     THE FIRST ANGLE FOLLOWS A COS-SIN DISTRIBUTION
    1 U1=RANF(N)
      U2=RANF(N)
      DEN=(2*U1-1)**2+U2**2
      IF (DEN .GE. 1) GO TO 1
      CPH=((2*U1-1)**2-U2**2)/DEN
      SPH=2*(2*U1-1)*U2/DEN
    2 U3=RANF(N)
      U4=RANF(N)
      IF (U3 .LT. U4) GO TO 2
      CTH=U3
      STH=SQRT(1-CTH**2)
      CA=CTH
      CB=STH*CPH
      CC=STH*SPH
      END
```

Appendix III: The Segment Approximation

Frequently, Knudsen flow occurs in tubes with very large length-to-radius ratios. Modeling this exactly requires an inordinate amount of computing time, so an approximation was devised. This is based on dividing the tube into 10 segments. For each segment, the following information is known:

a) Transmission factor--W

b) Average number of collisions for molecules that return--CR

c) Average number of collisions for molecules that escape--CE

If the reaction probability is RP, then the probability of no reaction is (1-RP). After m collisions, the probability of no reaction is $(1-RP)^m$. Thus, the average probability of reaction in a single segment is:

Molecule returns $PRR = 1 - (1-RP)^{CR}$

Molecule escapes $PRE = 1 - (1-RP)^{CE}$

These quantities are calculated at the beginning of the program and used when necessary.

A schematic flow chart is shown in Fig. 12. Initially, a random number is generated. If this random number is less than the Clausing factor for the segment, the molecule passes through that segment. Otherwise it returns. In this case, the probability of reacting on return, PRR, is called. A second random number is generated. If this random number is less than PRR, a reactive collision is recorded for segment 1. If this random number is greater than PRR, no reactive

collisions are recorded. After a molecule returns from segment 1, the program begins again with a new molecule.

Suppose, however, the molecule passes through segment 1. The probability of reacting on escape, PRE, is called. A random number is generated. As before, if this random number is less than PRE, a reactive collision is recorded for segment 1.

Now, the molecule passes on to segment 2. Once again it may either escape or return. As before, the possibility of a reactive collision in segment 2 is calculated. However, now if the molecule returns from segment 2 it may either escape from segment 1 or return from segment 1 and reenter segment 2.

If the molecule passes through segment 2, it enters segment 3. Thus, the program keeps adding segments. It should be noted that once a reactive collision occurs, the program begins again with another molecule. Due to the repetitive nature of the calculation, the program itself is quite straightforward.

For a tube with a length-to-radius ratio of 100, the approximation results were compared to results from the exact calculation. These were quite close. However, the approximation required only a fraction of the time the exact calculation required. A listing of the segment approximation program follows.

```
      PROGRAM RCOLL(INPUT, OUTPUT)
      DIMENSION RC(10)
      DO 900 I=1, 10
  900 RC(I)=0.
      P=1.0E-06
      LR=10000
      W=.00030
      CE=1.212223E+07
      CR=6.129410E+03
      I=0
C
C     CALCULATE PROBABILITY OF REACTING IF MOLECULE ESCAPES
      PRE=1-(1-P)**CE
C     CALCULATE PROBABILITY OF REACTING IF MOLECULE RETURNS
      PRR=1-(1-P)**CR
C
C     SEGMENT 1
    1 I=I+1
      IF (I .EQ. 10000001) GO TO 905
      R=RANF(N)
      IF (R .LT. W) GO TO 50
      RA=RANF(N)
      IF (RA .LT. PRR) RC(1)=RC(1)+1
      GO TO 1
   50 RA=RANF(N)
      IF (RA .LT. PRE) RC(1)=RC(1)+1
      IF (RA .LT. PRE) GO TO 1
C
C     SEGMENT 2
    2 R=RANF(N)
      IF (R .LT. W) GO TO 55
      RA=RANF(N)
      IF (RA .LT. PRR) RC(2)=RC(2)+1
      IF (RA .LT. PRR) GO TO 1
    3 R=RANF(N)
      IF (R .LT. W) GO TO 60
      RA=RANF(N)
      IF (RA .LT. PRR) RC(1)=RC(1)+1
      IF (RA .LT. PRR) GO TO 1
      GO TO 2
   60 RA=RANF(N)
      IF (RA .LT. PRE) RC(1)=RC(1)+1
      GO TO 1
   55 RA=RANF(N)
      IF (RA .LT. PRE) RC(2)=RC(2)+1
      IF (RA .LT. PRE) GO TO 1
C
C     SEGMENT 3
    4 R=RANF(N)
      IF (R .LT. W) GO TO 65
      RA=RANF(N)
      IF (RA .LT. PRR) RC(3)=RC(3)+1
      IF (RA .LT. PRR) GO TO 1
    5 R=RANF(N)
      IF (R .LT. W) GO TO 70
      RA=RANF(N)
      IF (RA .LT. PRR) RC(2)=RC(2)+1
      IF (RA .LT. PRR) GO TO 1
      GO TO 4
   70 R=RANF(N)
      IF (RA .LT. PRE) RC(2)=RC(2)+1
      IF (RA .LT. PRE) GO TO 1
```

```
      GO TO 3
   65 RA=RANF(N)
      IF (RA .LT. PRE) RC(3)=RC(3)+1
      IF (RA .LT. PRE) GO TO 1
C
C     SEGMENT 4
   6  R=RANF(N)
      IF (R .LT. W) GO TO 75
      RA=RANF(N)
      IF (RA .LT. PRR) RC(4)=RC(4)+1
      IF (RA .LT. PRR) GO TO 1
   7  R=RANF(N)
      IF (R .LT. W) GO TO 80
      RA=RANF(N)
      IF (RA .LT. PRR) RC(3)=RC(3)+1
      IF (RA .LT. PRR) GO TO 1
      GO TO 6
   80 RA=RANF(N)
      IF (RA .LT. PRE) RC(3)=RC(3)+1
      IF (RA .LT. PRE) GO TO 1
      GO TO 5
   75 RA=RANF(N)
      IF (RA .LT. PRE) RC(4)=RC(4)+1
      IF (RA .LT. PRE) GO TO 1
C
C     SEGMENT 5
   8  R=RANF(N)
      IF (R .LT. W) GO TO 85
      RA=RANF(N)
      IF (R .LT. PRR) RC(5)=RC(5)+1
      IF (RA .LT. PRR) GO TO 1
   9  R=RANF(N)
      IF (R .LT. W) GO TO 90
      RA=RANF(N)
      IF (RA .LT. PRR) RC(4)=RC(4)+1
      IF (RA .LT. PRR) GO TO 1
      GO TO 8
   90 RA=RANF(N)
      IF (RA .LT. PRE) RC(4)=RC(4)+1
      IF (RA .LT. PRE) GO TO 1
      GO TO 7
   85 RA=RANF(N)
      IF (RA .LT. PRE) RC(5)=RC(5)+1
      IF (RA .LT. PRE) GO TO 1
C
C     SEGMENT 6
   10 R=RANF(N)
      IF (R .LT. W) GO TO 95
      RA=RANF(N)
      IF (RA .LT. PRR) RC(6)=RC(6)+1
      IF (RA .LT. PRR) GO TO 1
   11 R=RANF(N)
      IF (R .LT. W) GO TO 100
      RA=RANF(N)
      IF (RA .LT. PRR) RC(5)=RC(5)+1
      IF (RA .LT. PRR) GO TO 1
      GO TO 10
   100 RA=RANF(N)
      IF (RA .LT. PRE) RC(5)=RC(5)+1
      IF (RA .LT. PRE) GO TO 1
      GO TO 9
   95 RA=RANF(N)
```

```
      IF (RA .LT. PRE) RC(6)=RC(6)+1
      IF (RA .LT. PRE) GO TO 1
C
C     SEGMENT 7
   12 R=RANF(N)
      IF (R .LT. W) GO TO 105
      RA=RANF(N)
      IF (RA .LT. PRR) RC(7)=RC(7)+1
      IF (RA .LT. PRR) GO TO 1
   13 R=RANF(N)
      IF (R .LT. W) GO TO 110
      RA=RANF(N)
      IF (RA .LT. PRR) RC(6)=RC(6)+1
      IF (RA .LT. PRR) GO TO 1
      GO TO 12
  110 RA=RANF(N)
      IF (RA .LT. PRE) RC(6)=RC(6)+1
      IF (RA .LT. PRE) GO TO 1
      GO TC 11
  105 RA=RANF(N)
      IF (RA .LT. PRE) RC(7)=RC(7)+1
      IF (RA .LT. PRE) GO TO 1
C
C     SEGMENT 8
   14 R=RANF(N)
      IF (R .LT. W) GO TO 115
      RA=RANF(N)
      IF (RA .LT. PRR) RC(8)=RC(8)+1
      IF (RA .LT. PRR) GO TO 1
   15 R=RANF(N)
      IF (R .LT. W) GO TO 120
      RA=RANF(N)
      IF (RA .LT. PRR) RC(7)=RC(7)+1
      IF (RA .LT. PRR) GO TO 1
      GO TO 14
  120 RA=RANF(N)
      IF (RA .LT. PRE) RC(7)=RC(7)+1
      IF (RA .LT. PRE) GO TO 1
      GO TC 13
  115 RA=RANF(N)
      IF (RA .LT. PRE) RC(8)=RC(8)+1
      IF (RA .LT. PRE) GO TO 1
C
C     SEGMENT 9
   16 R=RANF(N)
      IF (R .LT. W) GO TO 125
      RA=RANF(N)
      IF (RA .LT. PRR) RC(9)=RC(9)+1
      IF (RA .LT. PRR) GO TO 1
   17 R=RANF(N)
      IF (R .LT. W) GO TO 130
      RA=RANF(N)
      IF (RA .LT. PRR)  RC(8)=RC(8)+1
      IF (RA .LT. PRR) GO TO 1
      GO TO 16
  130 RA=RANF(N)
      IF (RA .LT. PRE) RC(8)=RC(8)+1
      IF (RA .LT. PRE) GO TO 1
      GO TO 15
  125 RA=RANF(N)
      IF (RA .LT. PRE) RC(9)=RC(9)+1
      IF (RA .LT. PRE) GO TO 1
```

```
C
C     SEGMENT 10
  18  PROB=1-(1-P)**2*LR
      RA=RANF(N)
      IF (RA .LT. PROB) RC(10)=RC(10)+1
      IF (RA .LT. PROB) GO TO 1
      R=RANF(N)
      IF (R .LT. W) GO TO 140
      RA=RANF(N)
      IF (RA .LT. PRR) RC(9)=RC(9)+1
      IF (RA .LT. PRR) GO TO 1
      GO TO 18
  140 RA=RANF(N)
      IF (RA .LT. PRE) RC(9)=RC(9)+1
      IF (RA .LT. PRE) GO TO 1
      GO TO 17
C
  905 CONTINUE
      PRINT 901
  901 FORMAT (*1*, *DISTRIBUTION OF REACTIVE COLLISIONS IN A CLOSED END
     1PORE*, ////)
      DO 910 J=1, 10
      PRINT 915, J, RC(J)
  915 FORMAT (* FOR SEGMENT *, I3, * NO. OF REACTIVE COLLISIONS = *,
     11PE13.05, /)
  910 CONTINUE
      END
```

555555555.555555555.555555555.555555555.555555555.555555555.555555555.555555555
555555555.555555555.555555555.555555555.555555555.555555555.555555555.555555555
555555555.555555555.555555555.555555555.555555555.555555555.555555555.555555555

References

1. A.D. Kirk, J. Chem. Ed. 44, 745 (1967).

2. M. Knudsen, Ann. Physik 28, 999 (1909).

3. P. Clausing, Ann. Physik 12, 961 (1932).

4. D.H. Davis, J. Appl. Phys. 31, 1169 (1960).

5. J.W. Ward, N.R. Mulford, and R.L. Bivins, J. Chem. Phys. 47, 1718 (1967).

6. J.W. Ward, J. Chem. Phys. 47, 4030 (1967).

7. J.W. Ward and M.V. Fraser, J. Chem. Phys. 49, 3743 (1968).

8. J.W. Ward, J. Chem. Phys. 49, 5129 (1968)

9. J.W. Ward and M.V. Fraser, J. Chem. Phys. 50, 1877 (1969).

10. J.W. Ward, R.L. Bivins, and M.V. Fraser, J. Vac. Sci. Technol. 7, 206 (1970).

11. J.W. Ward, M.V. Fraser, and R.L. Bivins, J. Vac. Sci. Technol. 9, 1056 (1972).

12. T.D. Sandry and F.D. Stevenson, J. Chem. Phys. 53, 151 (1970).

13. P. Clausing, Z. Physik 66, 471 (1930).

14. G.A. Somorjai, Chemistry in Two Dimensions: Surfaces, Cornell University Press, Ithaca, New York, 1981, p. 384.

15. D.J. Meschi and A.W. Searcy, unpublished work, 1980.

16. P.B. Weisz and C.D. Prater, Interpretation of Measurements in Experimental Catalysis, in Advances in Catalysis, Vol. 6, Academic Press, New York, 1954, pp. 143-196.

17. E. Kikuchi and Y. Morita, J. Catal. 15, 217 (1969)

18. T. Pignet and L.D. Schmidt, J. Catal. 38, 335 (1975).

19. E.W. Thiele, Ind. Eng. Chem. 31, 916 (1939).

20. C.N. Satterfield, Mass Transfer in Heterogeneous Catalysis, MIT Press, Cambridge, Massachusetts, 1970, pp. 128-134,

21. T.A. Nutall, Catalysts with Subsurface Active Layers Prepared by Co-impregnation, CSIR Report CENG 182, published by the Council for Scientific and Industrial Research, Pretoria, South Africa, 1977.

22. J. Cervello et al., Chem. Ing. Tech. 48, 520 (1976).

23. J. Wei and E.R. Becker, Adv. Chem. Series, No. 143, 116 (1975).

24. L.G. Loffler and L.D. Schmidt, J. Catal. 41, 470 (1977).

25. Op. cit., Somorjai, p. 445.

26. Op. cit., Somorjai, p. 418.

27. J.W. Evans, M.H. Abbasi, and A. Sarin, J. Chem. Phys. 72, 2967 (1980).

28. R.W. Hamming, Introduction to Applied Numerical Analysis, McGraw-Hill, New York, 1971, pp. 320-322.

29. J. von Neumann, National Bureau of Standards Applied Mathematics Series 12, 36 (1951).

Table 1. Average number of collisions per return, per escape, and per journey.

L/R	Average number of collisions per return	Average number of collisions per escape	Average number of collisions per journey
.01	1.0039	.0049	.0100
.02	1.0091	.0104	.0203
.03	1.0145	.0154	.0299
.04	1.0249	.0206	.0404
.05	1.0205	.0262	.0505
.06	1.0255	.0303	.0587
.07	1.0346	.0355	.0693
.08	1.0434	.0411	.0795
.09	1.0413	.0472	.0898
.10	1.0555	.0530	.1010
.20	1.0997	.1092	.1984
.30	1.1570	.1713	.2978
.40	1.2178	.2386	.3995
.50	1.2733	.3062	.4964
.60	1.3342	.3783	.5953
.70	1.4075	.4624	.7077
.80	1.4546	.5462	.8036
.90	1.5152	.6236	.8970
1.00	1.5856	.7174	1.0025
2	2.2376	1.7681	1.9955
3	2.9116	3.1210	2.9994
4	3.5655	4.7614	3.9913
5	4.2400	6.6468	4.9860
6	4.9022	8.9808	6.0256
7	5.5862	11.4432	7.0307
8	6.1716	14.0689	7.9362
9	6.8969	17.1245	9.0184
10	7.5545	20.4907	10.0341

Table 1. Continued

L/R	Average number of collisions per return	Average number of collisions per escape	Average number of collisions per journey
20	13.997	66.924	19.765
30	21.051	139.168	30.004
40	27.534	239.726	40.274
50	33.514	359.794	49.430
60	40.887	505.562	59.888
70	48.075	694.917	71.730
80	54.398	898.960	80.942
90	60.879	1107.554	90.018
100	66.251	1344.484	98.807
300	200	1.2307×10^4	298
500	399	3.4042×10^4	522
800	566	8.3059×10^4	831
1000	665	1.2400×10^5	984
3000	1.992×10^3	1.2439×10^6	3047
5000	$3.352.\times 0^3$	3.4716×10^6	5294
8000	5.786×10^3	7.7261×10^6	8642
10,000	6.129×10^3	1.2122×10^7	9764

Table 2: Collision Density along the Capillary Walls

Segment	Collisions from Monte Carlo calculation	Collisions from Clausing's calculation
1	1,865,262	1,846,857
2	1,663,729	1,656,539
3	1,460,141	1,466,220
4	1,274,694	1,275,902
5	1,070,316	1,085,583
6	877,480	895,265
7	702,557	704,946
8	513,313	514,628
9	324,771	324,309
10	128,461	133,991

Table 3: Closed End Pores (10^5 molecules)

L/R	Average number of collisions per journey	Number of collisions with pore bottom
1	2.0005	99,860
10	20.0586	101,446
50	99.5441	101,645
100	207.2713	105,709
200	405.4167	104,958

Figure Captions

Fig. 1 Flow regimes at T = 300°K.

Fig. 2 Collision density for an open end pore

L/R = 100 10^5 molecules.

Fig. 3 Collision density for a closed end pore

L/R = 100 49,573 molecules.

Fig. 4 Maximum depth of travel in a closed end pore.

L/R = 100 10^5 molecules.

Fig. 5 Proposed experiments for determining reaction probabilities.

Fig. 6 Distribution of reactive collisions in a closed end pore

L/R = 100 RP = 10^{-2} 10^5 molecules.

Fig. 7 Distribution of reactive collisions in a closed end pore

L/R = 10^5 RP = 3.3×10^{-3} 10^6 molecules.

Fig. 8 Distribution of reactive collisions in a closed end pore

L/R = 10^5 RP = 6.7×10^{-7} 10^6 molecules.

Fig. 9 Distribution of reactive collisions in a closed end pore

L/R = 10^5 RP = 5×10^{-9} 10^6 molecules.

Fig. 10 Derivation of sine-cosine distribution for θ.

Fig. 11. Derivation of distance, DW, from cylinder base to wall.

Fig. 12. Schematic flow chart of segment approximation program.

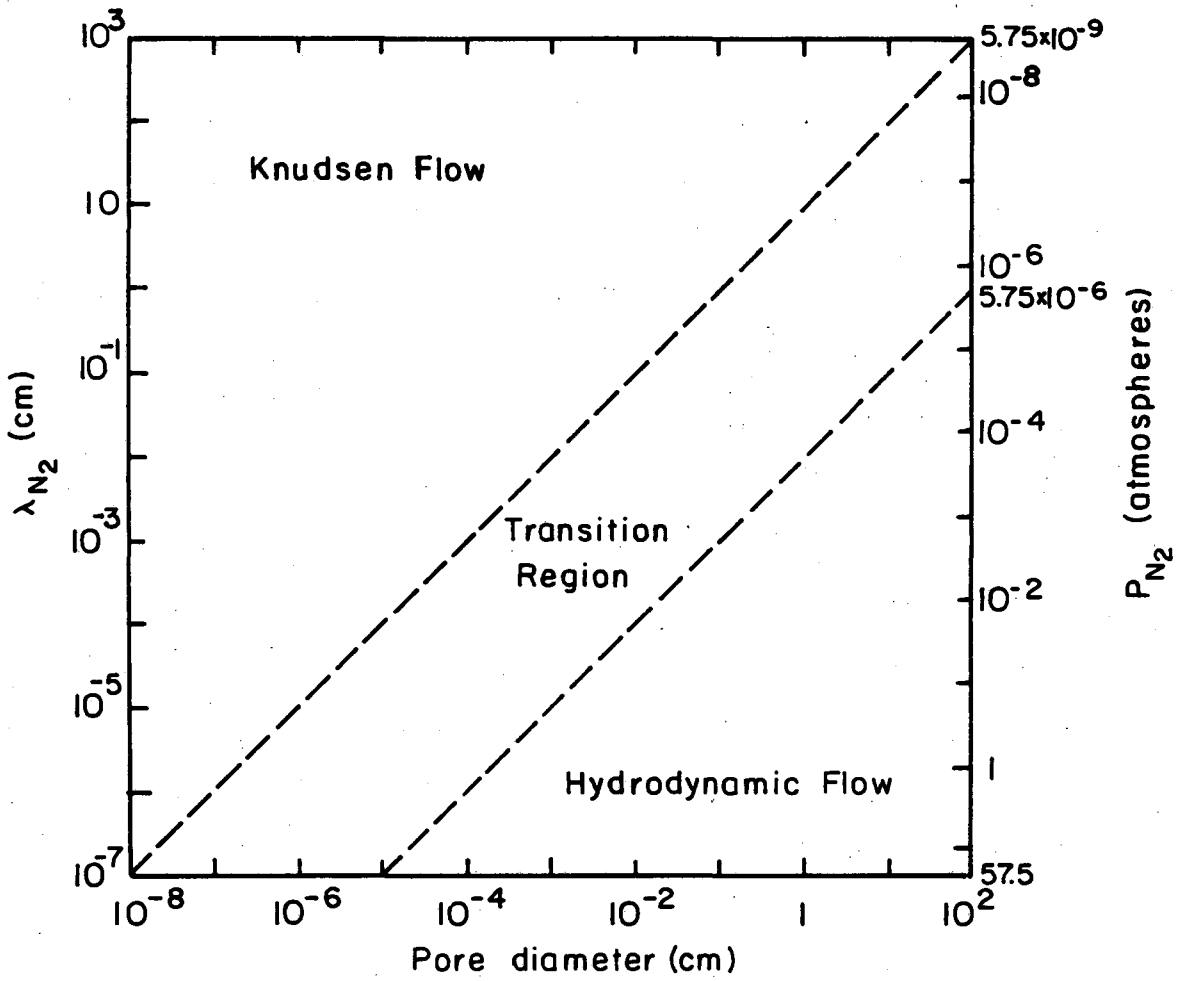

XBL 816-6015

Figure 1

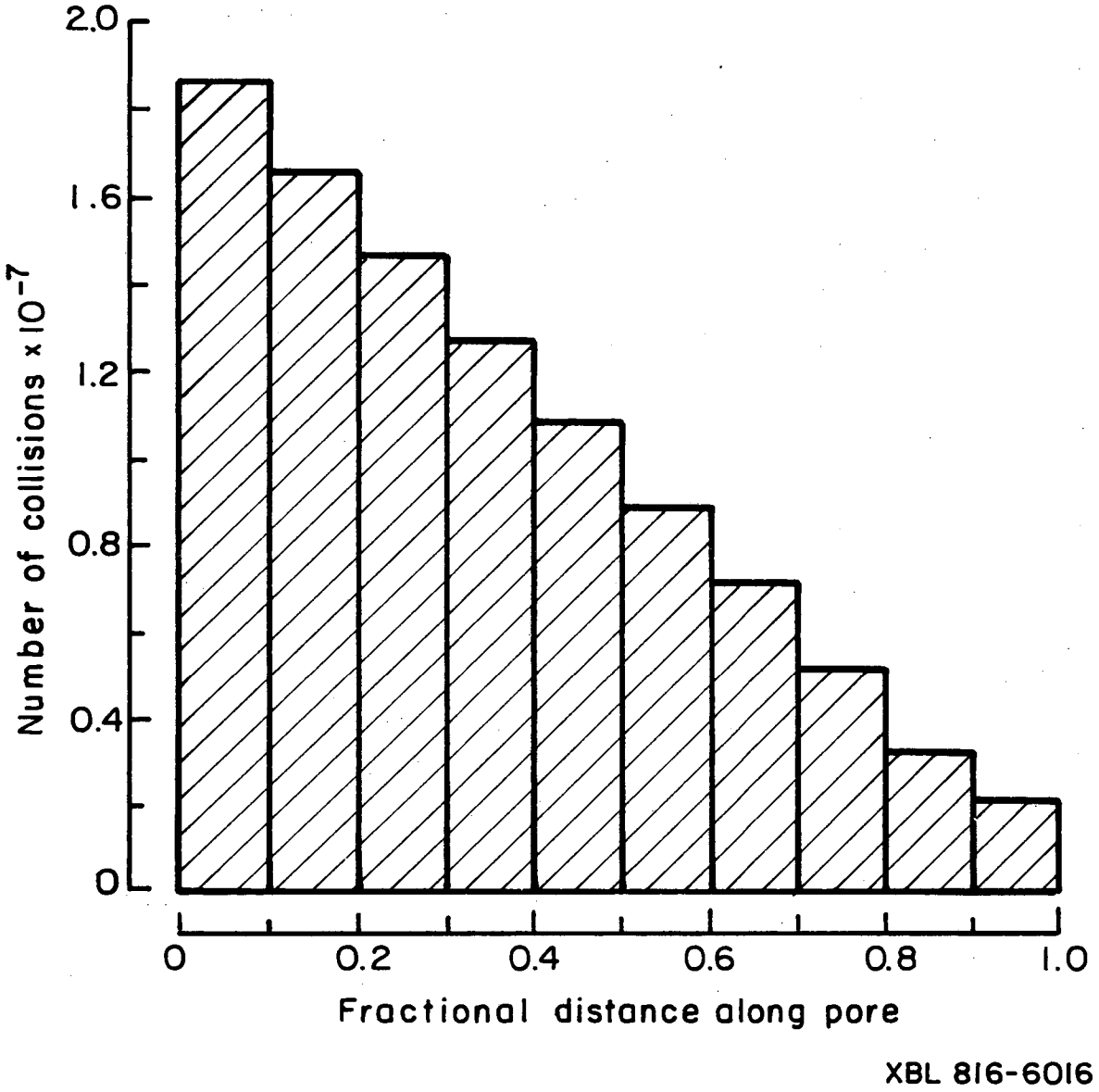
2.0
1.6
1.2
0.8
0.4
0
Number of collisions x 10^-7
0
0.2
0.4
0.6
0.8
1.0
Fractional distance along pore
XBL 816-6016

Figure 2

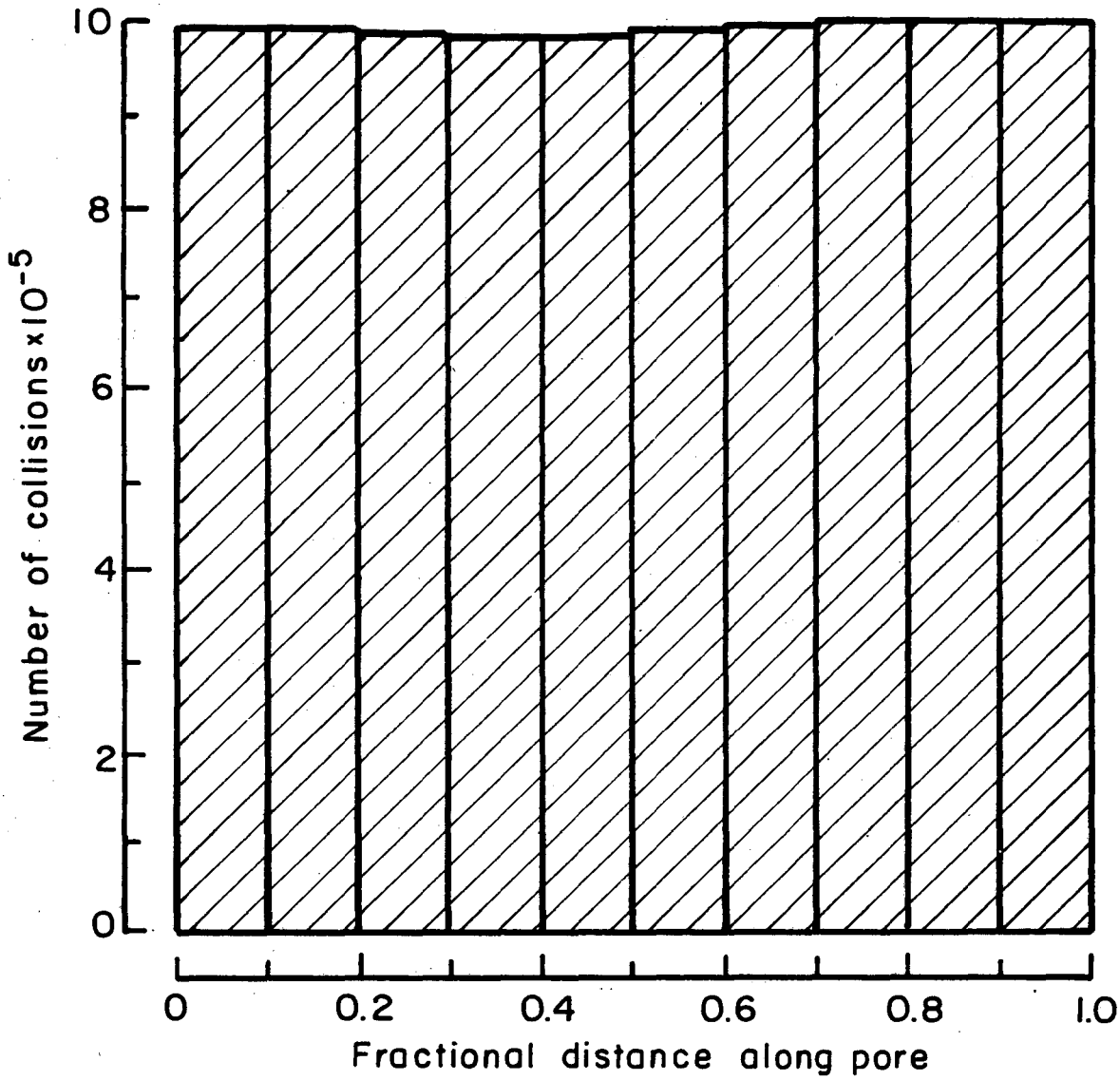

XBL 816-6017

Figure 3

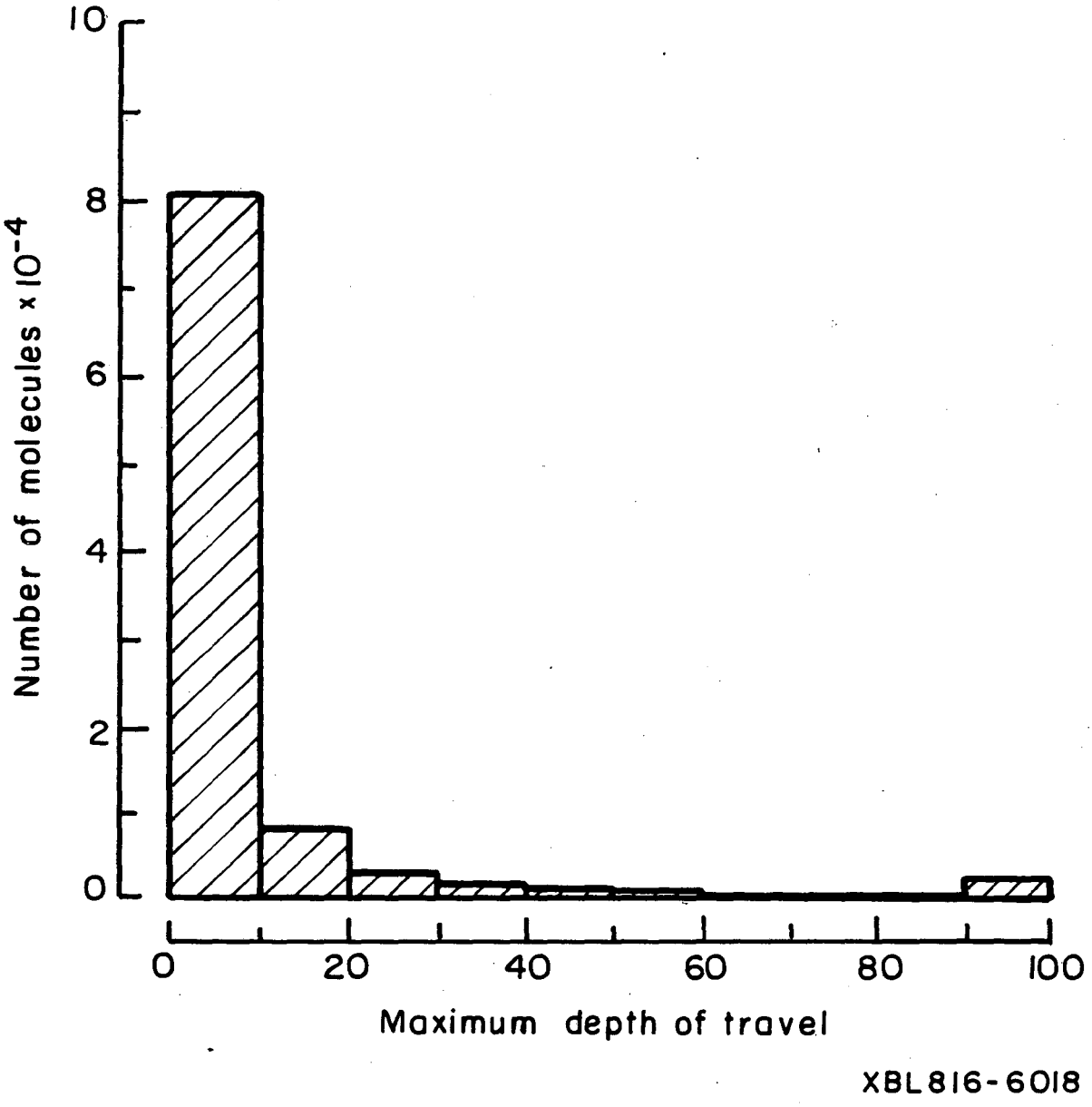
10
8
6
4
2
0
Number of molecules x 10^-4
0
20
40
60
80
100
Maximum depth of travel
XBL816-6018

Figure 4

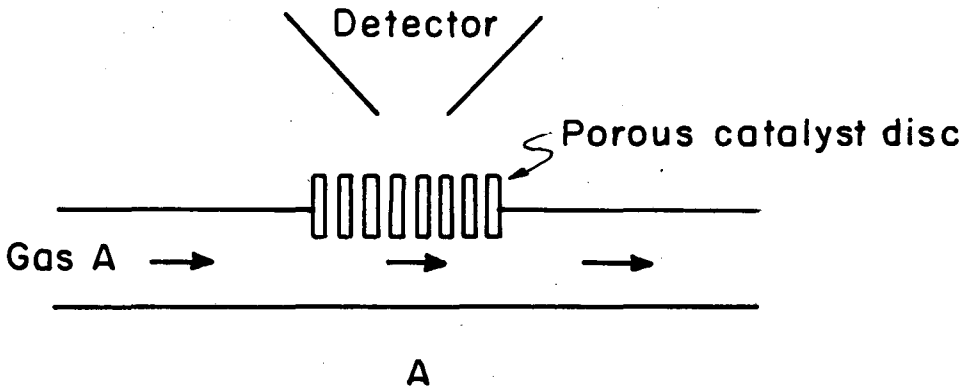

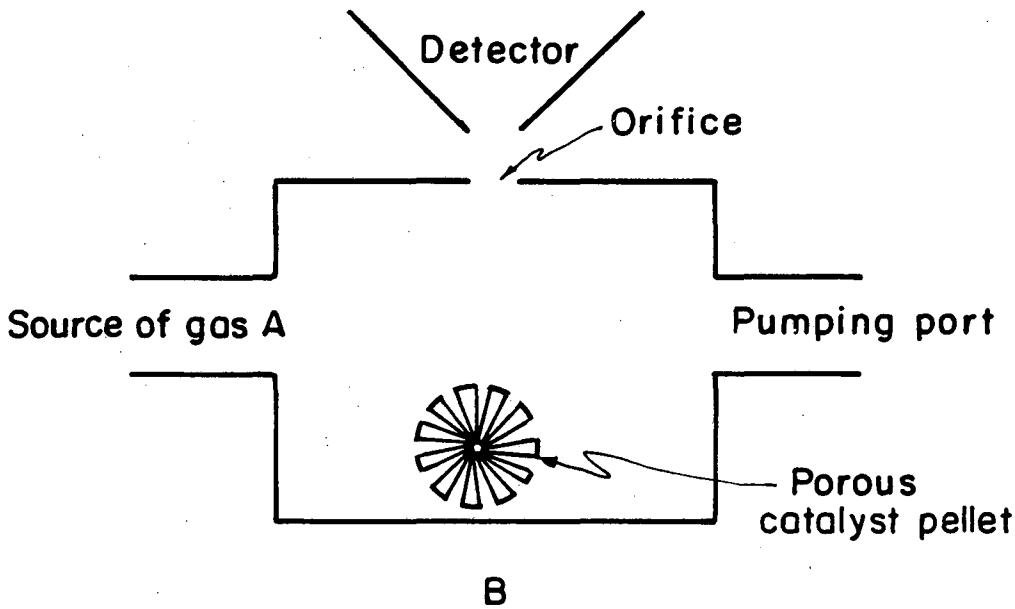

XBL 816-6019

Figure 5

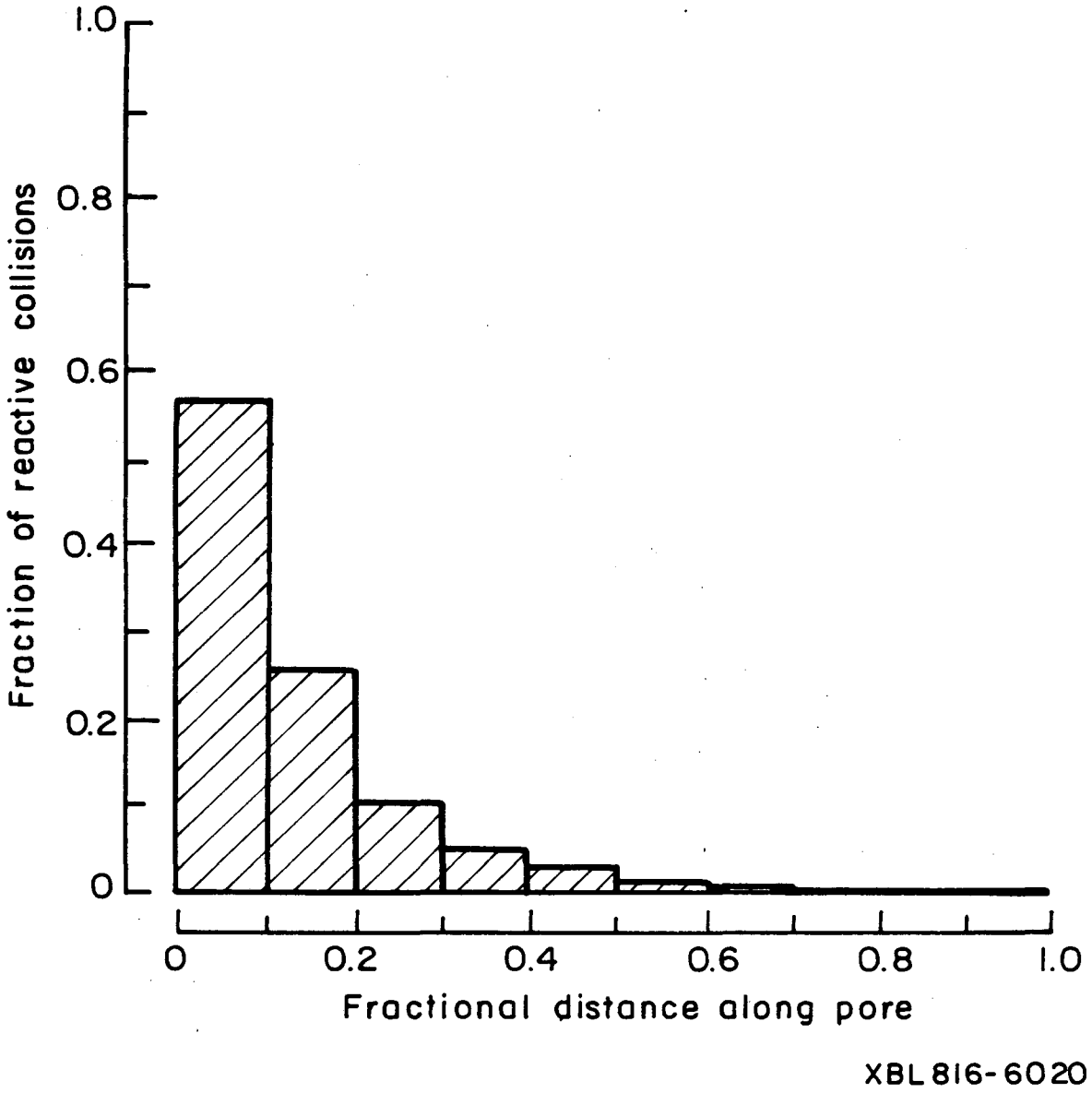
1.0
0.8
0.6
0.4
0.2
0
Fraction of reactive collisions
0
0.2
0.4
0.6
0.8
1.0
Fractional distance along pore
XBL 816-6020

Figure 6

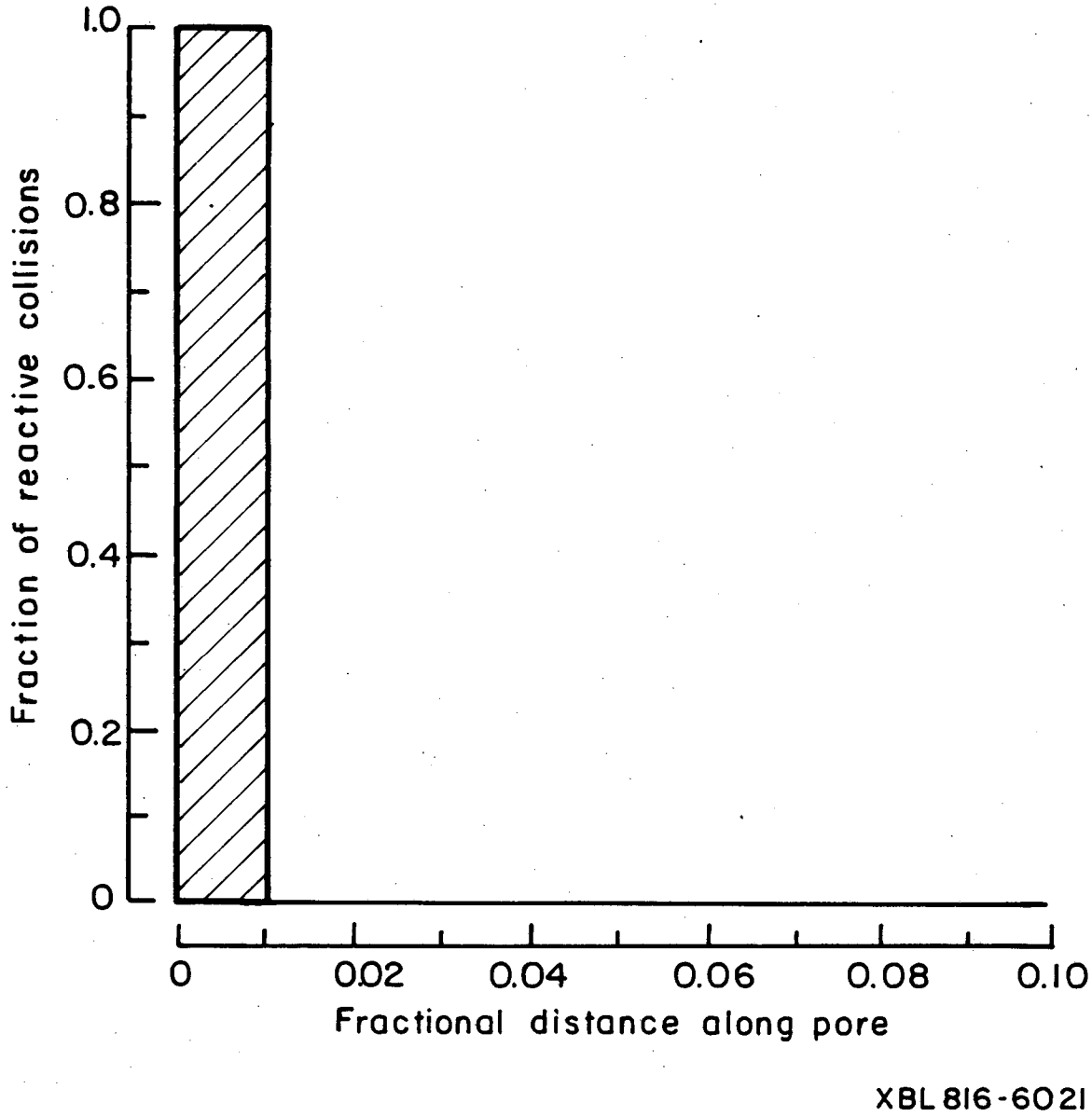
1.0
0.8
0.6
0.4
0.2
0
Fraction of reactive collisions
0
0.02
0.04
0.06
0.08
0.10
Fractional distance along pore
XBL 816-6021

Figure 7

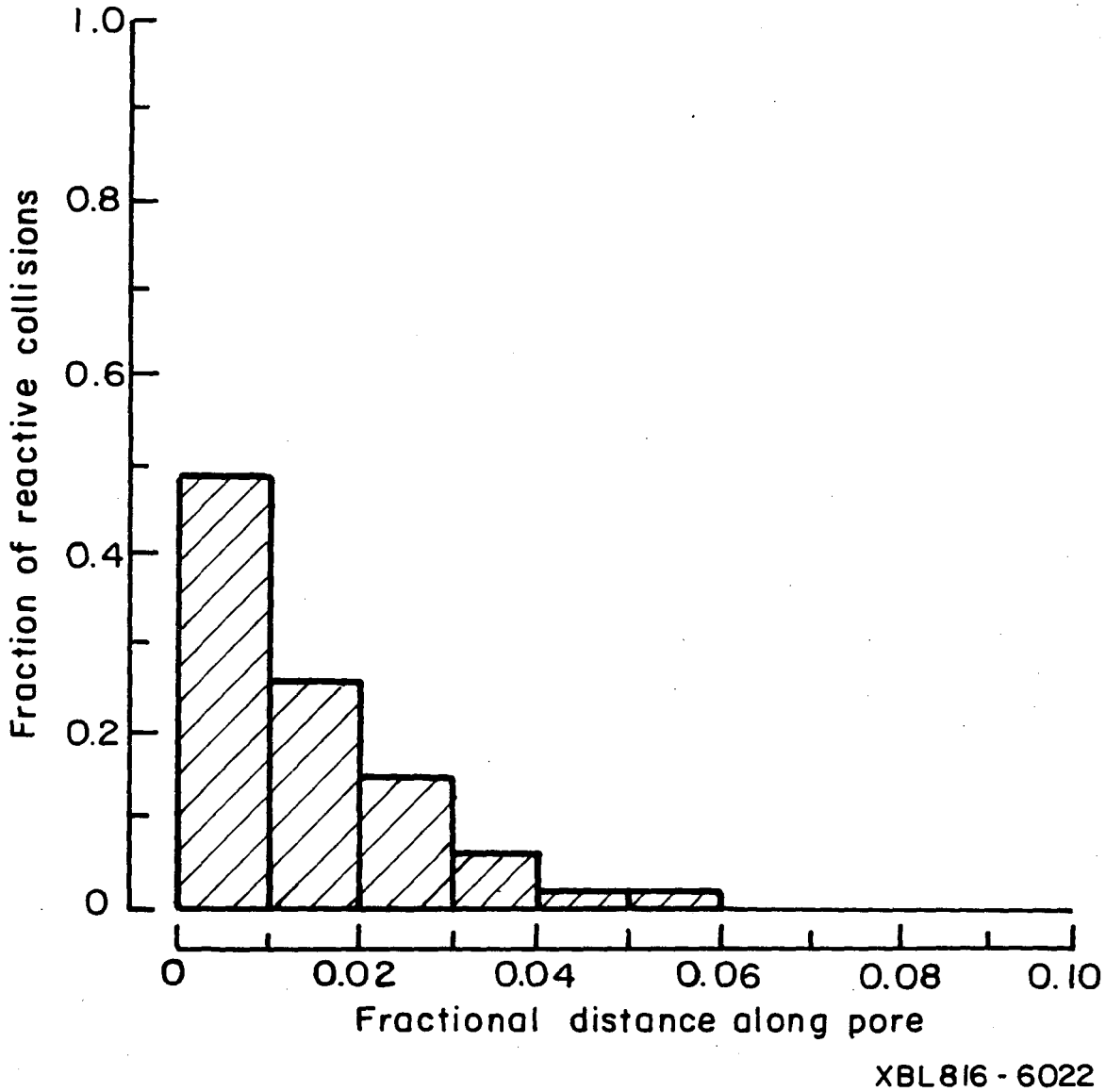
1.0
0.8
0.6
0.4
0.2
0
Fraction of reactive collisions
0
0.02
0.04
0.06
0.08
0.10
Fractional distance along pore
XBL816-6022

Figure 8

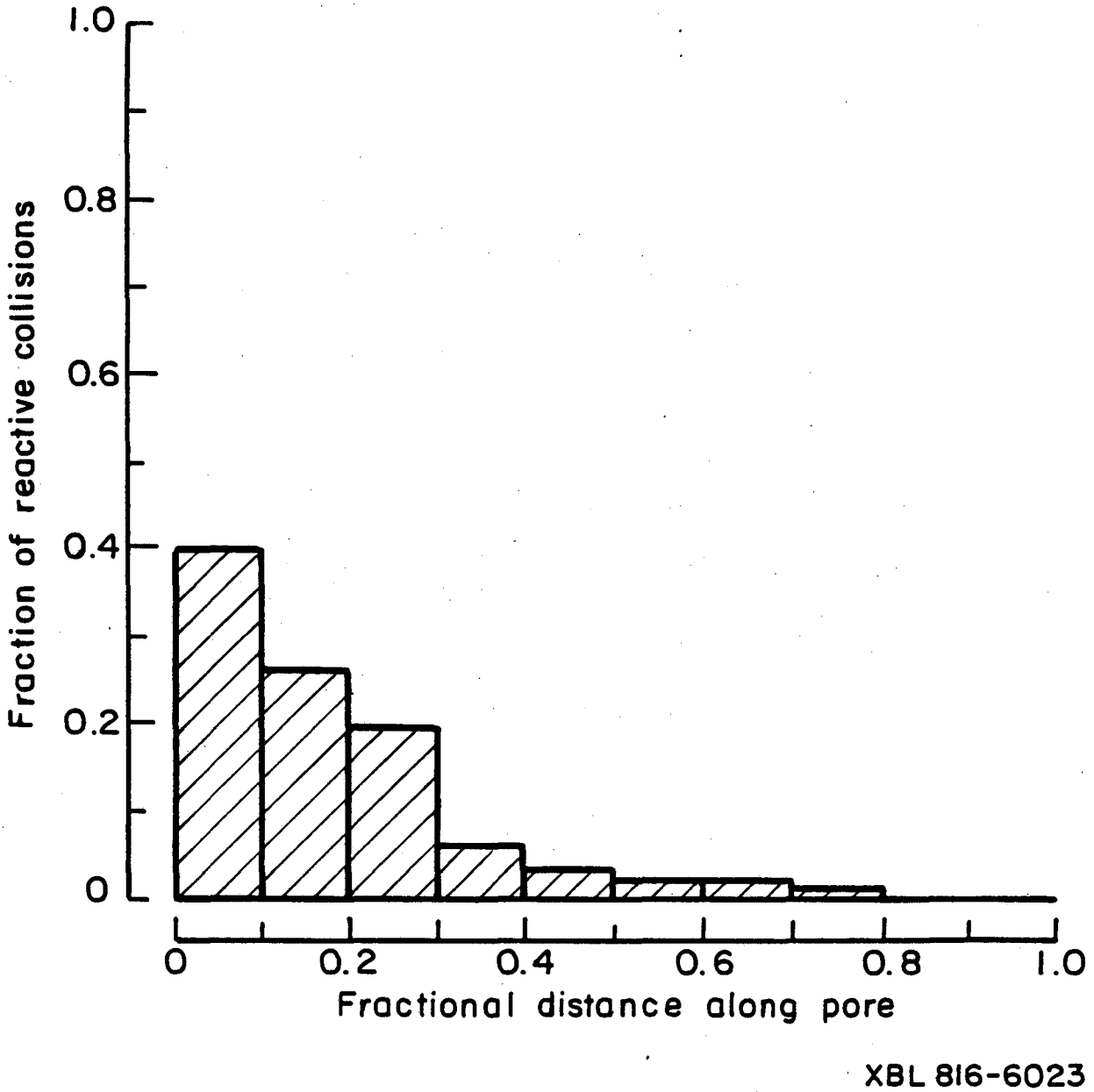
1.0
0.8
0.6
0.4
0.2
0
Fraction of reactive collisions
0
0.2
0.4
0.6
0.8
1.0
Fractional distance along pore
XBL 816-6023

Figure 9

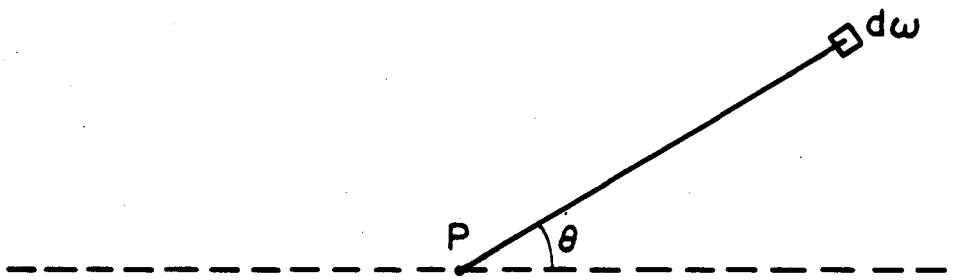

A Trajectory from a point P

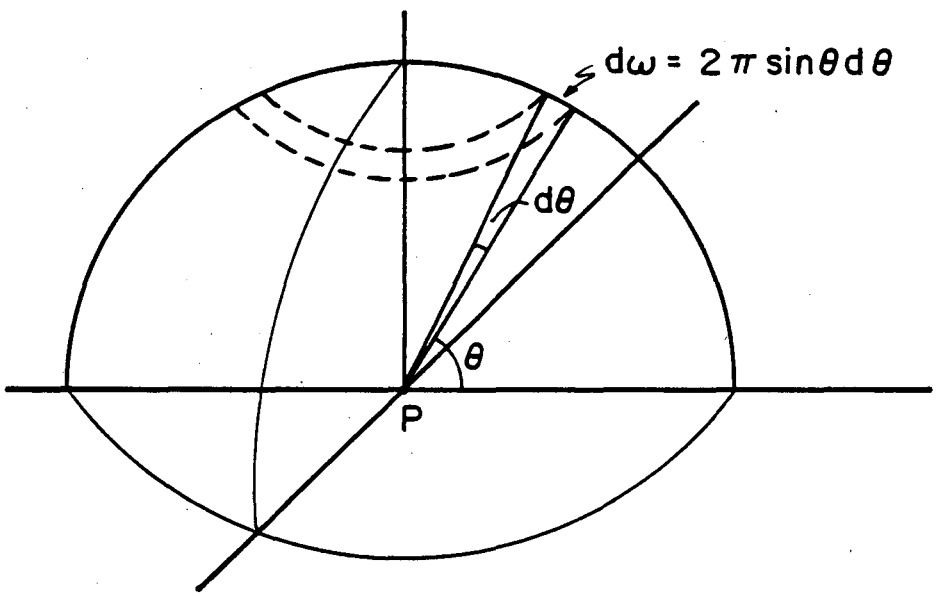

B Molecules leaving point P with angle θ pass into solid angle dω

XBL 816-6024

Figure 10

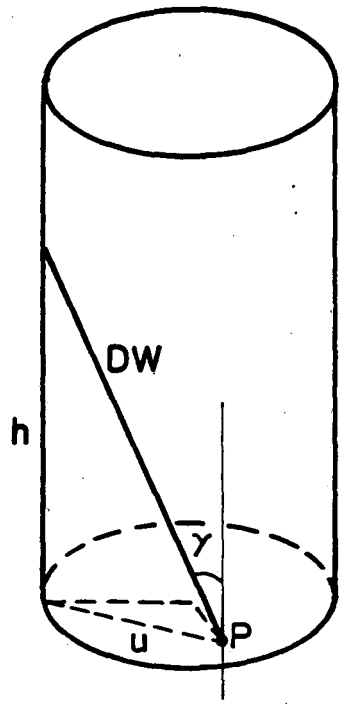

A Cylinder showing distance from starting point P to the wall

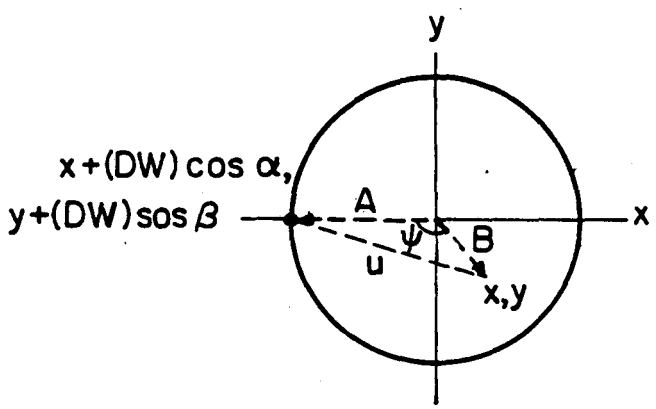

B Base of the cylinder

XBL 816-6025

Figure 11

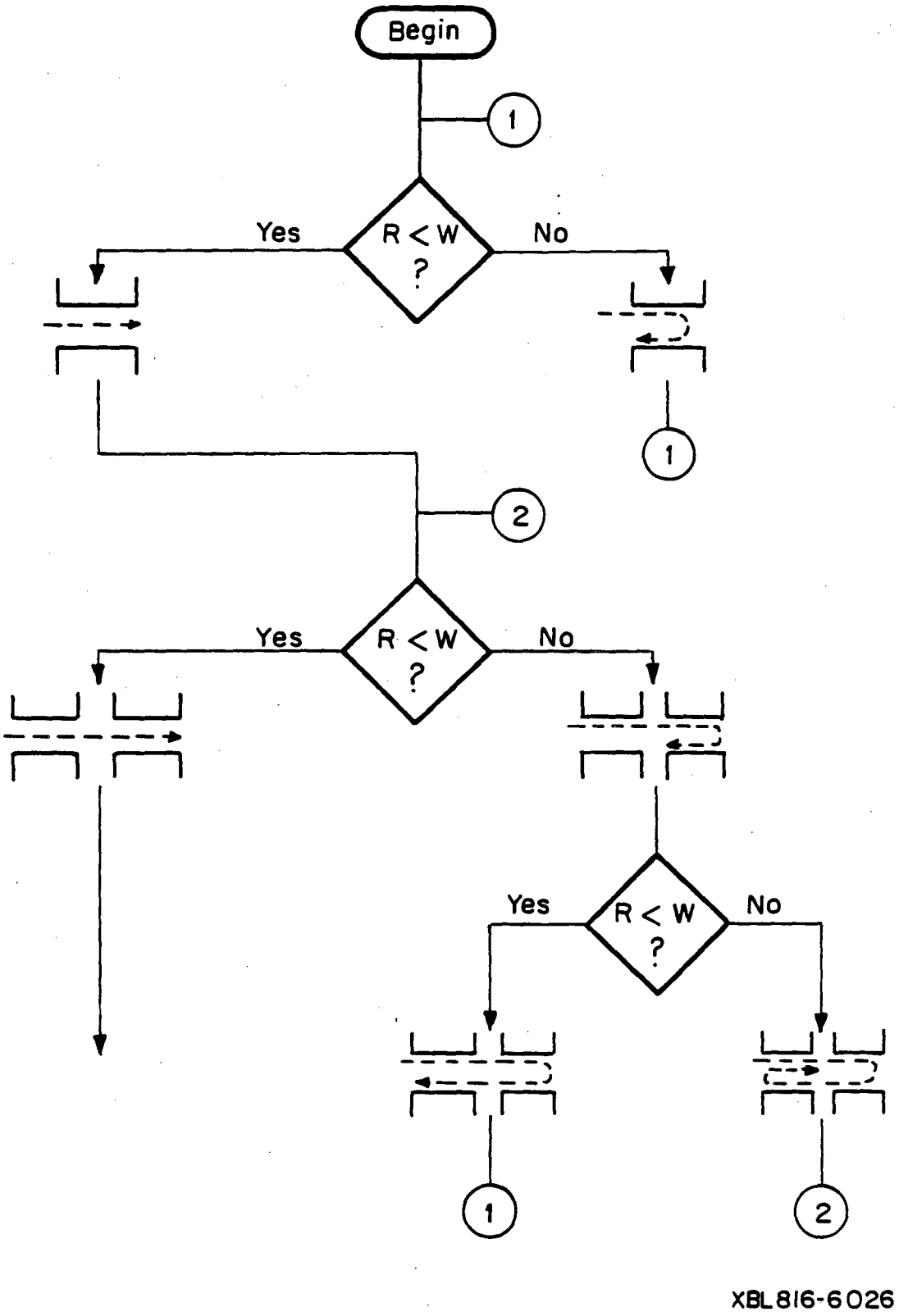

Figure 12

PART II. SURFACE DIFFUSION IN POROUS ALUMINA

1. Introduction

In Part I, molecular transport through tubes was described in terms of Knudsen flow. In pure Knudsen flow, a molecule strikes the wall of the tube, adsorbs, and immediately desorbs without movement on the surface. This simple behavior may not be exhibited if the molecule interacts with the wall. During adsorption, if the molecule is not held too tightly it can migrate along the surface. Thus, in a pressure gradient, a net surface flux develops, which is parallel to the Knudsen flux.

In this part of the thesis, the possibility of surface diffusion through porous solids is explored. Consider first the conditions that promote surface diffusion. The flux emerging from a pore is the sum of the Knudsen flux and the surface flux. The Knudsen flux density is in material per unit of pore cross-sectional area, and the surface flux density is in material per unit length of pore circumference. Assuming a cylindrical capillary, in order to normalize the surface flux it must be multiplied by the circumference of the capillary and divided by the area:

$$J_{total} = J_k + 2\pi r J_s/\pi r^2 = J_k + 2J_s/r$$

Thus, the surface flux component becomes larger with decreasing capillary radius. It is not possible to machine a capillary with a radius much less then 0.1 mm, so that to work with higher ratios of surface to

Knudsen flow a porous medium must be used. The high internal surface area of porous media can accommodate a larger population of adsorbed molecules and hence a larger surface diffusion contribution is expected. An example of a porous medium is a partially sintered powder compact. There are certain problems with porous media and they will be discussed later.

As mentioned, the diffusing molecule must interact with the capillary wall in order to diffuse on its surface. De Boer[1] gives, as the relationship between residence time on the surface and heat of desorption, $t = t_o e^{E/RT}$. Here, t is the time on the surface, t_o is a constant roughly equal to the vibrational period of an adsorbed molecule, E is the heat of desorption, R is the gas constant, and T is the temperature. This relationship is shown graphically in Fig. 13. For a large surface diffusion contribution, a high concentration of adsorbed molecules and a high surface mobility are required. Larger values of E/RT, and hence longer residence times, give high surface concentrations. However, since bonds must be broken or weakened for surface diffusion, smaller values of E/RT give a high surface mobility. Thus, there is very likely an intermediate value of E/RT that results in a maximum surface diffusion contribution. This maximum can be attained by either a small heat of adsorption (physical adsorption) and a low temperature, or a higher heat of adsorption and a higher temperature.

There is a large amount of literature on surface diffusion. Generally, this falls into three categories: First, there are studies of surface diffusion by gases through porous media at low temperatures.

These studies are found throughout the chemical engineering literature; a summary is provided in the first chapter of Satterfield's book.[2] In the field of high temperature science, a number of investigators have concerned themselves with possible errors in effusion studies due to surface diffusion through the orifice of a Knudsen cell. Their work is summarized in a recent review article by Cater.[3] Finally, many researchers have examined the surface diffusion of simple gas molecules on single crystals, as well as the surface self-diffusion of metals, in an attempt to gain a mechanistic understanding of surface diffusion. They use the many available surface techniques; their work is summarized in a review by Ehrlich and Stolt.[4]

Consider first the work on porous media at lower temperatures. At room temperature, the diffusing gas need only show a weak interaction with the surface in order to surface diffuse. Thus, gases such as carbon dioxide, nitrogen, and even xenon may exhibit surface diffusion in porous media at room temperature. For helium, however, surface diffusion is known to be negligible at room temperature because it is adsorbed to only a small degree.[5] Consequently, helium is used as a standard for nonadsorbed flow.

Barrer is one of the most prolific investigators in this area.[6-9] Most of his studies are on carbon powder compacts with pore diameters of about 20 nm or less. He measured the permeabilities of these compacts to various gases. Permeability is defined as $K = Jl/(A\Delta c_g)$. Here J is the flux in molecules per second emerging from the porous plug, l is the thickness of the plug, A is the

cross-sectional area of the plug, and Δc_g is the concentration drop between the entrance and exit of the plug. The measured permeability is the sum of the Knudsen flow and surface flow permeabilities: $K = K_g + K_s$. The Knudsen flow component is calculated from helium measurements: $K_g = K^{He} \sqrt{M_{He}/M}$, where M is the molecular weight. Thus, surface permeability can be calculated from $K_s = K - K_g = K - K^{He} \sqrt{M_{He}/M}$. For carbon dioxide through a carbolac plug,[8] Barrer et al. measure K_s/K_g equal to 6.8 at 308°K. At 378°K, this value decreases to 3.3. This is due to the net decrease in surface carbon dioxide concentration.

Barrer views the surface flux as arising from a submonolayer film. The molecules in this layer undergo a random walk, like a two-dimensional gas.

Not all investigators interpret their results this way. Gilliland et al.[10] have measured the flow of various gases through porous vycor. They observe ethylene, propylene, and isobutane to pass through vycor up to seventeen times faster than nonadsorbed gases. They cannot reconcile this dramatic result with submonolayer coverage. Instead, they develop a theory based on a spreading film.

The studies discussed so far deal with low temperatures and low heats of adsorption. As pointed out earlier, surface diffusion may also occur at high temperatures and higher heats of adsorption. For example, barium atoms have been observed to migrate on a tungsten surface at 900°K.[11] Apparently, the surface diffusion of high temperature vapors through porous media has not been studied. However, some researchers

have examined how surface diffusion might alter the apparent vapor pressures measured from effusion cells.

Equilibrium pressures derived from effusion studies usually assume that Knudsen flow is the primary mechanism of transport through the orifice. This may not always be the case. Hirth and Winterbottom[12-14] have developed a theory for combined surface flow and Knudsen flow through short cylindrical and conical orifices. They propose that surface diffusion can increase the net flux emerging from the orifice in three ways: (a) migration along the cell lid bottom to the orifice, (b) migration along the orifice walls, and (c) migration out of the orifice along the cell lid top. They begin with the continuity condition $-\nabla \cdot J_S = J_V - J_I$, which they assume must be satisfied at any element of area on the cell surface. These fluxes have the following definitions:

$$J_S = \text{surface flux} = -D_S \nabla n(x)$$

$$J_V = \text{desorption flux} = n(x)\alpha = n(x)\alpha_o \exp(-E_{des}/RT)$$

$$J_I = \text{impinging flux} = n_e\alpha.$$

Here $n(x)$ is the concentration of adsorbed molecules and n_e is the concentration of adsorbed molecules in equilibrium with the vapor. To solve these equations for the surface diffusion contribution, the values of the surface diffusion coefficient--D_S, the energy of desorption--E_{des}, and the evaporation probability--α_o are required. Generally, these quantities are unavailable. However, Winterbottom and Hirth used data for silver vapor on nickel and molybdenum surfaces to support their theoretical conclusion that the greatest surface diffusion

contribution is expected for small orifice diameters, small length-to-radius or knife edge orifices, and higher temperatures. Ward et al.[15,16] have done computer simulations of Knudsen and surface diffusion through orifices, which yield results similar to those of Winterbottom and Hirth.

Actual evidence for surface diffusion in effusion cells is limited. Boyer and Meadowcroft[17] have measured the free energy of vaporization of silver, under conditions Winterbottom and Hirth predict will promote surface diffusion. Use of a molybdenum cell lid with a small diameter knife edge orifice yields an apparent $\Delta G_0 = 54{,}400-20.4T$. When corrected for surface diffusion, the data becomes much closer to the accepted value of $\Delta G_0 = 63{,}600-26.23T$. The difference between the apparent value of ΔG_0 and the accepted value becomes much less for larger orifice diameters. Grimley et al.[18] have observed altered angular distributions of samarium vapor emerging from tantalum and boron nitride orifices. They attribute this to bulk diffusion in the orifice walls.

The surface effects modeled by Winterbottom and Hirth for a Knudsen cell arise primarily from end effects. In a porous plug, these end effects would not be expected to contribute significantly to the total flux. However, the porous plug would have a larger adsorbed population on the internal pore walls. This adsorbed population could contribute the total flux substantially, as demonstrated by Barrer at lower temperatures.[8]

Related to high temperature surface diffusion is the phenomenon of "orifice creep," or "bulk surface flow." These terms describe the creep of large amounts of material up the walls of the cell and out of the orifice. This phenomenon has been mentioned by several investigators.[3,19] It has been observed with CrF_3, CoF_2, and FeF_2 on alumina cells in this laboratory.[20]

Steady-state surface diffusion is generally described by Fick's first law: $J_S = -D_S(dc_s/dx)$. Here J_S is a flux in mole/(cm sec), D_S is a surface diffusion coefficient in cm^2/sec, and c_S is a surface concentration in moles/cm^2. Because surface diffusion is an activated process involving the breaking and making of bonds, D_S varies exponentially with temperature:

$$D_S = A \exp(\Delta S^*/R) \exp(-\Delta H^*/RT)$$

ΔS^* and ΔH^* are the entropy and enthalpy of activation for surface diffusion. ΔH^* must, of course, be less than the heat of desorption. Satterfield states that it is generally about one-half the heat of desorption[21] for physically adsorbed molecules. D_S can be regarded as a measure of surface mobility, whereas t, the residence time, is related to surface concentration:

$$C_S = B \exp(-\Delta S_d/R) \exp(\Delta H_d/RT).$$

Here, ΔS_d and ΔH_d are the entropy and enthalpy of desorption. The gas phase concentration is included in B. As mentioned, there is probably some optimum combination of the surface mobility and surface concentration that gives a maximum surface flux.

The actual mechanism of surface diffusion is not well understood. For low surface concentrations, one can envision a random hopping of molecules with each jump from one to several atomic spacings. The surface diffusion coefficient for such a process is given by $D_S = a^2/4t$,[22] where a is the average displacement and t is the average time per jump. For a high surface concentration, the motion of atoms is correlated, and calculation of the diffusion coefficient becomes more complex.

In this study, several of the techniques used by previous investigators are combined to study surface diffusion. Porous alumina was chosen as the solid. Helium and a variety of permanent gases are shown to pass through this material primarily by Knudsen flow. High temperature vapors that are likely to interact with an alumina surface are also passed through the porous alumina. Several of these vapors show significant surface diffusion. Temperature dependence measurements and Auger measurements reveal some information on the nature of this high temperature surface diffusion.

Throughout this study, transmission probabilities are used to describe diffusion. If only Knudsen flow is important, these probabilities are independent of vapor molecule, solid, and temperature. For surface diffusion, this need not be the case. Thus, a Knudsen flow

transmission probability is predicted and measured with helium. Larger transmission probabilities are attributed to surface diffusion.

2. Characterization of Porous Alumina

Porous alumina was chosen as the solid porous medium to study. Many supported catalysts are on porous alumina substrates. Elucidating the transport properties in these substrates is important in understanding catalysis. In addition, alumina is an important high-temperature material--effusion cells are often constructed of alumina. Therefore, understanding possible surface interactions of high-temperature vapors with alumina is important. Finally, porous alumina is relatively easy to fabricate.

The porous alumina was used in the form of barriers 1.024 ± 0.004 mm thick. These were made at the LBL ceramics shop from an alumina greenware, which is a mixture of approximately micron-sized alumina particles (99.5 percent pure) and a resin binder. The mixture was fired at about 1250°C for roughly one hour. This procedure left a partially sintered porous product. Several samples were characterized in order to be certain that different samples had similar porosities and pore diameters.

Two samples were examined with a mercury porosimeter; the results are shown if Figs. 14 and 15. Both samples have similar properties. These measurements show that most of the penetration occurs at pressures corresponding to pore diameters of 1.1 to 0.6μ. From the penetration volume, the relative porosity ε can be calculated:

$$\varepsilon = \frac{\text{Volume of pores in 1 gr}}{\text{Total volume of 1 gr}}$$

$$= \frac{\text{Penetration volume per gram}}{\text{Penetration volume per gram + volume of solid per gram}}$$

The volume of solid per gram is simply the inverse of the density of dense alumina. Both samples had a relative porosity of 0.45.

The relative porosity was also measured directly. A block of precise dimension was cut, thoroughly dried, and weighed. The weight-to-volume ratio gave a density of 2.13 gr/cc. The density of dense alumina is 3.97 gr/cc. The relative porosity was calculated as follows:

$$\varepsilon = \frac{\text{Volume of pores in 1 gram}}{\text{Total volume of 1 gram}}$$

$$= \frac{1/2.13 - 1/3.97}{1/2.13} = .46$$

The average of these three porosity values is .453 ± .006.

The surface area of five samples was measured with a BET apparatus. This gave an average value of .61 ± .11 m^2/gr. Typically, surface area measurements below 1 m^2/gr are not very accurate, so these measurements show good agreement. This indicates that different samples have similar porosities and pore sizes. The low surface area also rules out the possibility of a second distribution of smaller pores.

The average pore diameter can also be estimated from these surface area and density measurements.[23] Consider the porous material to be a bundle of n parallel capillaries with radius r and length l. The volume of the pores divided by their surface area gives the average pore radius: $r/2 = n\pi r^2\, l/(2\pi r\, l) = V_p/S$. V_p is the volume of pores per gram and S is the surface area per gram. The external surface area is negligible compared to the internal surface area of the pores. V_p can be calculated from the relative porosity and density. The relative porosity is $\varepsilon = V_p/(V_p + V_S)$. V_s is the volume of solid per gram $1/\rho$, where ρ is the density of dense alumina. Thus, the pore volume is $V_p = (\varepsilon/1-\varepsilon)\, 1/\rho$. Putting this into the expression for pore radii gives:

$$r = \frac{2}{S}\,\frac{\varepsilon}{1-\varepsilon}\,\frac{1}{\rho} \qquad\qquad d = \frac{4}{S}\,\frac{\varepsilon}{1-\varepsilon}\,\frac{1}{\rho}$$

d is the pore diameter. The mean pore diameter calculated from the average surface area is $1.2 \pm 0.2\mu$.

A third way of estimating pore diameters is from direct observation with a scanning electron microscope. Figure 16 shows a general micrograph of the porous alumina. Figure 17 shows a more detailed micrograph. Each crack and crevice was measured in this micrograph, and the average pore diameter was determined to be $0.9 \pm 0.4\mu$. Given the irregular shapes of the pores, these three methods

of estimating pore diameters show very good agreement. The average of the three gives the average pore diameter as $1.0 \pm 0.3\mu$.

The micrographs show the porous material is not a bundle of parallel capillaries, but rather a network of randomly oriented pores. These pores may be of nonuniform diameter, multiply bent, and cross linked. There may also be dead end pores.[24] These deviations from ideality reduce experimental transmission probabilities below those predicted for a bundle of parallel capillaries with the same surface area and pore volume.

The tortuosity factor, τ , is used to correct for these deviations from ideality. For a straight cylindrical tube with a length-to-radius ratio of 100 or greater, the transmission probability is $4/3\ d/l$.[25] For a porous barrier this becomes $1/\tau\ (4/3)\ (d/l)$, where τ generally varies from 1 to 10.[26] Putting these values for τ , the average pore diameter, and the barrier thickness into this equation gives transmission probabilities of $(1.3\text{-}13) \times 10^{-4}$. Helium should have a transmission probability in this range. Gases for which surface diffusion is important should show larger transmission probabilities.

3. Experimental

Two systems were constructed for measuring transmission probabilities of gases through porous barriers. One was for measurements of permanent gases such as helium and nitrogen, and the other was for measurements of high temperature vapors such as zinc vapor and lithium fluoride vapor. Both systems had a reversible gas source, so that

molecules that did not pass through the barrier could not build up a large pressure at the entrance side of the barrier.

The apparatus for studying permanent gases is shown in Fig. 18. It consisted of a gas manifold with high vacuum valves constructed of teflon with viton O-rings. Cylinders of various gases could easily be connected to this manifold. Tygon tubing between the gas cylinder and the manifold introduced impurities, so stainless steel lines were used instead. The manifold itself contained a large bulb, a thermocouple to measure the gas temperature, and a capacitance manometer connected to a strip chart recorder. A mullite tube, mounted on a large flange, was connected to the manifold. This flange was mounted in a high vacuum chamber. The mullite tube had a rather thick wall--0.32 ± .01 cm--and an inside diameter of 1.06 ± .01 cm. This tube had a smooth ground end on which a flat porous alumina barrier was placed. Over the barrier was a spring-loaded cap. This arrangement was designed to make the leakage path as long as possible, thus minimizing escape other than through the barrier.

In order to measure transmission probabilities, the volume of the manifold up to the barrier must be known. To measure this volume, the system was valved off right before the barrier. Then a known volume of gas at about 5×10^2 Pa was expanded into the system. The volume of the manifold was calculated from $V_2 = P_1V_1/P_2$. The volume from the valve near the barrier to the barrier was estimated and added to V_2. The total volume of the manifold was determined to be 4.4 ± 0.1 liters.

Transmission probabilities were calculated from the rate of gas leakage through the barrier into the high vacuum. Initially, the manifold was filled to about 14 Pa pressure. Then it was opened to the porous barrier. The rate of leakage from the gas bulb is simply the time derivative of the ideal gas law: $dn/dt = (V/RT_m)\, dP/dt$. The flow rate through the porous barrier is given by the Hertz-Knudsen-Langmuir equation modified by the transmission probability, W:

$$J = \frac{1}{A}\frac{dn}{dt} = \frac{WP}{\sqrt{2\pi MRT_b}}$$

Equating these two expressions and integrating gives the expression for the transmission probability:

$$W = \frac{\sqrt{2\pi MRT_b}}{A_p}\,\frac{V}{RT_m}\,\frac{\Delta \ln P}{\Delta t}$$

M = Molecular weight of the diffusing gas

R = Gas constant

A_p = Exposed area of the barrier fronted by pores

= (exposed area)(porosity) = 0.41 ± .02 cm^2

V = Volume of the manifold to the barrier

T_b = Temperature of the gas in the barrier

T_m = Temperature of the gas in the manifold

$\Delta \ln P/\Delta t$ = The rate of leakage from the bulb.

The rate of leakage was calculated from the output of the capacitance manometer, which was on a strip chart recorder. The logarithms of about 20 pressure points were taken. These quantities, together with the corresponding times, were analyzed with a least-squares method to obtain a slope.

In order to check this method, argon was passed through a dense alumina disc with an effusion orifice which had a helium transmission probability of 0.36. The measured transmission probability was 0.32 ± .01, showing good agreement.

Eight gases were examined using this technique. Before introducing a new gas, the system was evacuated, filled with the new gas, and then evacuated again. Four measurements were taken for each gas--two with one barrier and two with another barrier of the same thickness.

The other class of gases studied was high temperature vapors. An apparatus similar to that of Mohazzabi[27] was used. This is shown in Fig. 19. Mohazzabi found that lithium fluoride passed through cell walls of dense alumina at elevated temperatures, so boron nitride was used instead of alumina for the cell body. Thick-walled cells were used for both mechanical strength and for a better seal between the cell body and cell lid. As before, the leakage path was made as long as possible to minimize any leakage. Boron nitride cell lids with 0.50 ± 0.02 mm diameter orifices as well as porous alumina cell lids were machined to fit the cells. The entire assembly was surrounded by a molybdenum jacket.

This assembly was heated with a tungsten furnace wound on an alumina form. One thermocouple was pinned to the furnace for temperature

control. Another thermocouple was pinned to the bottom of the molybdenum jacket for cell temperature measurement. The temperature inside the cell was calculated from a weight loss technique. This temperature was about 50°K hotter than the temperature measured at the bottom of the molybdenum jacket.

The cell assembly was positioned so that no condensation occurred on the lid. This was done by moving the cell assembly in the furnace to a point where the lid gained no weight during an experiment. This means the cell lid was hotter--perhaps by as much as 20°K--than the cell bottom. However, results indicate the measured transmission factors were not strongly temperature dependent.

Escape fluxes of the high temperature vapors were measured using a standard weight loss technique. First, the cell, cell lid, and solid to be vaporized were weighed. Then this assembly was loaded into the vacuum furnace chamber. The furnace had a ramp controller, so the cell was rapidly brought up to temperature (~10°K/min). A timer was then started and the cell left at temperature from 8 to 15 hours. At the end of a run, the furnace was shut off and the timer stopped. After cooling, the cell, lid, and remaining solid were weighed again. In order to minimize hydration problems, the cell, lid, and solid were thoroughly baked out. In subsequent measurements, the same cell, lid, and solid were used. A minimal amount of time was taken for removing the cell assembly from the vacuum chamber and weighing it.

The flux emerging from the orifice or barrier was calculated from the weight loss as follows:

$$J\left(\frac{\text{mole}}{\text{cm}^2\ \text{sec}}\right) = \frac{\Delta w}{MtA_{eff}}$$

Δw is the weight loss, t is the time at temperature, and A_{eff} is the effective area. For an orifice this is simply the measured area, and for a porous barrier this is the area fronted by pores; i.e., the exposed area multiplied by the porosity. M is the molecular weight of the effusing vapor. For zinc this is simply the atomic weight. However, the alkali halides vaporize as both monomers and dimers, so it is more complicated. For an orifice, M is the average molecular weight of the equilibrium vapor calculated from the fractional fluxes and monomer and dimer molecular weights. This average was calculated from data in the JANAF thermochemical tables.[28] Mohazzabi and Searcy[29] have shown that, for sodium chloride, porous barriers like those of this study shift the monomer-dimer equilibrium to yield only traces of dimer. So, for a porous barrier experiment, M is the molecular weight of the monomer. Both orifice and porous barrier flux densities are expressed in equivalent monomer units; i.e., $J_M + 2\ J_D$ where J_M is the monomer flux and J_D is the dimer flux.

Zinc and three alkali halide salts--sodium chloride, sodium fluoride, and lithium fluoride--were examined. Reagent grade chemicals were used for each. These materials all have vaporization coefficients of one,[30] indicating they are a reversible source of vapor molecules.

The orifice measurements gave the equilibrium fluxes. In order to determine the temperature inside the cell, these fluxes were compared

to a computer-calculated listing of flux, $J = P/\sqrt{2\pi MRT}$ $= e^{\Delta S_v/R}\, e^{-\Delta H_v/RT}/\sqrt{2\pi MRT}$, and corresponding temperature. Here ΔS_v and ΔH_v are the entropy and enthalpy of vaporization.

Due to the unit vaporization coefficient, equilibrium pressures are established in the cells, and this flux was also the flux, J_o, impinging on the bottom of the barrier. The porous barrier measurements gave the flux, J_L, leaving the barrier. Transmission probabilities were then calculated from these two quantities: $W = J_L/J_o$. Several measurements were taken for each vapor.

The vacuum chamber used for both the permanent gas and high temperature vapor measurements was the Knudsen cell chamber of a Nuclide model HT-12-60 mass spectrometer. The temperature dependence of the effusing vapors could be determined using the mass spectrometer. In a mass spectrometer, ion intensity, I, and temperature, T, are related to partial pressure by $P = KIT/\sigma$.[31] Here K is a constant characteristic of the machine and σ is the ionization cross section of the particular vapor molecule. Thus, when ion intensities are measured as a function of temperature, a plot of ln IT vs 1/T yields an enthalpy from the slope. For Knudsen effusion, this quantity is the enthalpy of vaporization. When surface diffusion is important, this quantity reflects a weighted average of the enthalpy of vaporization and enthalpy of adsorption and surface diffusion.

There was some concern about a possible reaction between the alumina barrier and the fluoride salts. Therefore, after an experiment the remaining solid and the barrier were examined with a Picker powder

diffractometer. The porous alumina barrier is a collection of randomly oriented crystallites, so it yielded a powder pattern when placed directly in the x-ray stage.

Lithium fluoride showed a major surface effect. Therefore, the surfaces of a barrier, through which lithium fluoride had diffused, were examined with a Perkin-Elmer Scanning Auger Microscope in order to gain information on the surface layer.

4. Results and Discussion

Table 4 lists the transmission probabilities for eight permanent gases at room temperature. Helium has a transmission probability in the range predicted for Knudsen flow. This result indicates that there are no major leaks in the system and that helium does indeed pass through the barrier entirely by Knudsen flow. This is expected, since helium should show little or no interaction with the solid surface. Helium will be used as a standard for Knudsen flow throughout this study. The measured transmission probability for helium should be independent of temperature. It can be used to calculate the tortuosity factor of the porous alumina from $\tau = (4/3)(d/l)/W_{HE}$. This gave a value of $\tau = 2.0 \pm 0.3$.

Table 4 also lists the transmission factors for Ar, N_2, CO_2, O_2, CH_4, NH_3, and SO_2. These are all approximately the same as helium. Thus, it can be concluded that these gases all pass through the barrier by Knudsen flow. Other investigators have reported that these gases physically adsorb and surface diffuse on porous silica and carbon,

with pores 1-20 nm in diameter, at room temperature.[8,10] Since physical adsorption is nonspecific, one might expect similar behavior here. The reason it is not observed is very likely due to the larger pores in our material (~10^3 nm). If the surface diffusion flux is inversely proportional to the radius, increasing the pore size two orders of magnitude would certainly remove any surface diffusion contribution.

Table 5 compares the transmission probabilities measured for helium and four high temperature vapors. Zinc vapor has a transmission probability close to that of helium, indicating that there are no major leaks in the system and that Knudsen flow is the primary means of transport through the barrier. However, the alkali halide salt vapors show larger transmission probabilities. These can only be attributed to adsorption and subsequent migration along the pore surfaces. The ratio of Knudsen flux to surface flux, also in Table 5, was calculated from $(J_L - W_{He}J_o)/W_{He}J_o$. Here J_L is the total flux leaving the barrier, W_{He} is the transmission probability for helium, and J_o is the flux incident on the barrier.

Mohazzabi and Searcy[29] have shown that the monomers and dimers of sodium chloride vapor equilibrate in a porous alumina barrier. These experiments were in the Knudsen flow regime, which means very few gas-phase collisions. Since equilibrium is dynamic, equilibration must be occurring in a surface layer. It is not surprising that some transport is occurring in this layer.

However, Mohazzabi and Searcy also report that zinc and sodium chloride exhibit similar transmission probabilities. They used a porous

alumina with pores ~5μ in diameter. If the surface diffusion coefficient is inversely proportional to the pore radius, J_s/J_k would be ~0.3, which may not be a measurable effect.

Mohazzabi[27] found that a .838 mm thick porous barrier shifted the sodium chloride monomer to dimer ratio, from approximately 2.5 at the barrier's entrance to approximately 130 at the barrier's exit at 1025°K. This was an expected result of equilibration in a pressure gradient, and can be predicted by solving the simultaneous equations for monomer flux, J_M, and dimer flux, J_D:

$$J_D/J_M^2 = K_p(\pi\ MRT)^{1/2} \qquad J_M + 2\ J_D = J_L$$

Here, K_p is the pressure equilibrium constant for the monomer-dimer reaction, M is the molecular weight of the monomer, and J_L is the total flux leaving the barrier in equivalent monomer units. A similar measurement was taken for lithium fluoride through a 1 mm thick barrier at 1115°K. Here, the monomer-to-dimer ratio shifted from about .7 at the entrance to about 12 at the exit. Although this is not as dramatic as the sodium chloride effect, it still roughly agrees with the predictions of the above equations, indicating equilibration occurs in the barrier. It is quite likely that the monomers and dimers of all alkali halides will equilibrate in such a porous alumina barrier. As mentioned, this must be occurring on the surface. Thus, surface transport for lithium fluoride and sodium fluoride was also expected.

There was some concern that these salt vapors might react with the alumina. Free energy calculations indicate the reaction of NaF and Al_2O_3 to form Na_2O and AlF_3 is not favorable under these conditions. The formation of cryolite, Na_3AlF_6, does have a standard free energy of -161 Kcal/mole at 1100°K:

$$12\ NaF(g) + Al_2O_3(s) \rightarrow 2\ Na_3AlF_6(s) + 3\ Na_2O(s)$$

However, this corresponds to an equilibrium vapor pressure for NaF of 2×10^{-3} atm. Since the pressure in the cell was never greater than 10^{-5} atm, this reaction is not important. There was also no physical evidence of a reaction occurring to any large extent. After an experiment, the barrier gained about a milligram weight compared to a total weight loss of five milligrams or more of sodium fluoride. X-raying the used barrier showed only alumina peaks. X-raying the remaining solid showed only sodium fluoride peaks.

A similar situation exists with lithium fluoride and alumina. The formation of Li_2O and AlF_3 is energetically unfavorable. A lithium fluoride aluminate has been reported, but it is formed under very high pressures.[32] The formation of the lithium analog of cryolite, Li_3AlF_6, does have a standard free energy of -583 + .361T Kcal/mole in this temperature range:

$$12\ LiF(g) + Al_2O_3(s) \rightarrow 2\ Li_3AlF_6(l) + 3\ Li_2O(s)$$

This corresponds to an equilibrium lithium fluoride pressure well above that in the cell, so this reaction cannot occur. Similarly, the reaction to form Li_3AlF_6 and Li_2O gas cannot occur to any appreciable extent with this low vapor pressure of lithium fluoride. As before, there was no physical evidence of a reaction between the vapor and the barrier. After an experiment, the barrier gained less than a milligram in weight compared to a total weight loss of five milligrams of lithium fluoride. The barrier showed x-ray peaks of only alumina and the remaining solid showed only lithium fluoride peaks. A used barrier was sectioned and examined with an Auger spectrometer. This showed a small amount of fluorine at the entrance to the barrier, but no detectable amounts at the interior.

Reaction of sodium chloride with alumina cannot be important, since the formation of Na_3AlCl_6 is energetically unfavorable under these conditions. Thus, none of the alkali halide vapors examined form a compound with the alumina. However, they do interact with the alumina enough to form a mobile surface layer.

In order to gain more information on the nature of the adsorbed layer, the temperature dependence of the flux leaving the barrier was measured with the mass spectrometer. As mentioned in the experimental section, a plot of ln IT vs 1/T gives an enthalpy, which reveals something about the vaporization and diffusion processes. If surface diffusion is important, there are four major steps: vaporization from the solid, adsorption on the alumina, surface migration on the alumina, and desorption from the alumina. The measured heat should be the

difference between the enthalpy of the solid and the enthalpy of the activated state of the slowest step. One might expect the slowest step to be desorption. If the vapor molecule is held tightly to the solid it is diffusing on, the measured enthalpy will probably be lower than the enthalpy of vaporization. This might be the reason Boyer and Meadowcroft[17] measured a lower heat when silver vapor surface diffuses through a molybdenum orifice. However, if the vapor molecule is weakly bound to the solid, the measured enthalpy could be about the same as the enthalpy of vaporization.

Measurements for sodium chloride are shown in Figs. 20 and 21; measurements for lithium fluoride are shown in Figs. 22 and 23. In both cases, only the principal peak was examined--Na^+ or Li^+. These are the most intense peaks, and are at low enough mass numbers so that they are not masked by any hydrocarbon peaks. Consider first the measurements below the melting point. All four figures have orifice measurements on them for reference--this is the heat of vaporization. The porous barrier measurements give heats very close to these. This suggests the sodium chloride vapor molecule and lithium fluoride vapor molecule are very loosely bound to the alumina pore surface.

The behavior above the melting point is more complex. Consider first sodium chloride. Figure 20 shows that, at the melting point, the flux through the barrier on a boron nitride cell shows a dramatic increase. A discontinuity such as this suggests a change in diffusion mechanisms--very likely to the surface-creep mechanism discussed in the introduction.

In order to determine if this is an effect of the cell wall material, an alumina cell with a porous barrier was also examined. The results are shown in Fig. 21. Here, the expected results were obtained--a small bending over at the melting point. However, in earlier experiments, when the porous barrier was colder than the rest of the cell, a melting point transition to this surface-creep mechanism was observed with alumina cells. Thus, the appearance of this mechanism is a function of both cell material and the presence of thermal gradients.

For lithium fluoride, something else is occurring. This is shown for both a boron nitride cell and an alumina cell in Figs. 22 and 23. In both cases the flux increases more rapidly after the melting point. A possible explanation for this is that, after melting, the vapor forms a monolayer that penetrates further into the barrier. Thus, the effective barrier thickness decreases and the emerging flux increases. This is a phenomenon that requires more investigation.

Note that for lithium fluoride in an alumina cell a transition --presumably to the surface-creep mechanism--occurs well above the melting point. This contrasts with sodium chloride in a boron nitride cell. As mentioned in the introduction, this type of mechanism has been observed by other investigators. It can be a major problem in effusion studies, so that understanding when and why it occurs would be of great value, but the behavior above the melting point is evidently complex and further studies in that range were not made part of the present work.

In order to gain more information about the adsorbed layer of lithium fluoride, several used barriers were examined with an Auger

spectrometer. Since the lithium and aluminum peaks overlap, only the fluorine peak was examined. Very small amounts of fluorine were found at the entrance side of some barriers. Other barriers showed no detectable fluorine there. No barriers showed detectable fluorine on the exit side. Two barriers were sectioned and no fluorine was found in the interior. The limits of detection of this spectrometer is about one atomic percent in a disk .2 to 1μ in diameter and ~20 Å deep. Thus, a dilute monolayer would not be detectable, but a multimolecular layer should be.

The Auger results, together with the temperature dependence measurements, suggest that the surface contributions are due to loosely bound, dilute monolayers--like a two-dimensional gas. This is an interpretation similar to Barrer's for surface diffusion of gases such as CO_2 or xenon on carbons.[8]

This study can be regarded as a synthesis of the work of Winterbottom and Hirth on effusion cells and the work of Barrer on porous media. Winterbottom and Hirth treat the surface diffusion of high temperature vapors as a hindrance to effusion studies, and attribute to it enhanced fluxes from the bottom of a cell lid into the orifice channel and from the orifice channel onto the outer lid surface. Here surface diffusion of high temperature vapors is treated as an interesting phenomenon in itself. It is studied under conditions somewhat like those used by Barrer for lower temperature studies of surface diffusion--a porous barrier with a high surface area to volume ratio. Here surface diffusion cannot be attributed to end effects, but rather the presence of

a loosely bound, dilute adsorbed layer on the pore walls. For alkali metal halides, surface diffusion on alumina proves to be measurable when pores are ~1 μm in diameter. Barrer found similar surface flux to Knudsen flux ratios for permanent gases, but with pores 20 nm or less in diameter.

5. Conclusions

It has been shown that a combination of small pores and an appropriate gas-solid interaction will promote surface diffusion of alkali halide vapors in porous media. A variety of gases and vapors were passed through porous alumina barriers 1.024 ± .004 mm thick, with pore diameters of 1.0 ± 0.3μ. Helium showed the transmission probability predicted for Knudsen flow, indicating it could be used as a standard. Ar, N_2, CO_2, O_2, CH_4, NH_3, and SO_2 all showed behavior similar to that of helium, indicating that they pass through this material by Knudsen flow at room temperature. At 630°K, zinc vapor also passes through these barriers by Knudsen flow. However, three alkali halide salt vapors--sodium chloride, sodium fluoride, and lithium fluoride--were shown to pass through the barrier at 2.6 to 9.8 times the rate expected for Knudsen flow, indicating the presence of a mobile surface layer. Apparently, this is the first dramatic evidence of surface diffusion at high temperatures in porous media. Temperature dependence experiments and Auger examination of used barriers suggest the surface layer is a loosely bound, dilute monolayer.

The use of porous barriers in conjunction with high temperature vapors appears to be a promising method to investigate the surface interactions of these vapors. This work suggests a number of possible studies. The behavior of porous alumina and lithium fluoride above the melting point merits further investigation. It would also be interesting to vary the barrier material. In light of previous studies, silver vapor on porous molybdenum should show a substantial surface component.

References

1. J.H. de Boer, The Dynamical Character of Adsorption, Oxford University Press, London, 1953, p. 35.
2. C.N. Satterfield, Mass Transfer in Heterogeneous Catalysis, MIT Press, Cambridge, Massachusetts, 1970, pp. 1-77.
3. E.D. Cater, The Effusion Method at Age 69: Current State of the Art, NBS Special Publication 561, 1979, pp. 10-13.
4. G. Ehrlich and K. Stolt, Surface Diffusion, in Ann. Rev. Phys. Chem. Vol. 131, 1980, pp. 603-637.
5. Op. cit. Satterfield, p. 48.
6. R.M. Barrer, Surface and Volume Flow in Porous Media, in The Solid Gas Interface, Vol. 1, M. Dekker, New York, 1967, pp. 557-609.
7. R.M. Barrer and T. Gabor, Proc. Roy. Soc. (London), A251, 353 (1959).
8. R. Ash, R.M. Barrer, J.H. Clint, R.J. Dolphin, and C.L. Murray, Roy. Soc. (London) Phil. Trans. 275, 255 (1973).
9. R.M. Barrer, Diffusion in and Through Solids, Cambridge University Press, London, 1951.
10. E.R. Gilliland, R.F. Baddour, and J.L. Russell, A.I.Ch.E. Journal 4, 90 (1958).
11. Op. cit. de Boer, p. 93.
12. W.L. Winterbottom and J.P. Hirth, J. Chem. Phys. 37, 784 (1962).
13. W.L. Winterbottom, J. Chem. Phys. 47, 3546 (1967).
14. D.L. Dunham and J.P. Hirth, J. Chem. Phys. 49, 4650 (1968).

15. J.W. Ward, R.L. Bivins, and M.V. Fraser, J. Vac. Sci. Technol. 7, 206 (1970).

16. J.W. Ward, M.V. Fraser, and R.L. Bivins, J. Vac. Sci. Technol. 9, 1056 (1972).

17. A.J. Boyer and T.R. Meadowcroft, Trans. Met. Soc. AIME 233, 388 (1965).

18. R.T. Grimley, L.C. Wagner, and P.M. Castle, J. Appl. Phys. 46, 4090 (1975).

19. J.W. Ward and M.V. Fraser, J. Chem. Phys. 50, 1877 (1969).

20. M. Huang, D.J. Meschi, and A.W. Searcy, unpublished work, 1976.

21. Op. Cit. Satterfield, p. 49.

22. J.C. Tully, G.H. Gilmer, and M.H. Shugard, J. Chem. Phys. 71, 1630 (1979).

23. Op. Cit. Satterfield, p. 41.

24. D. Nicholson and J.H. Petropoulous, Capillary Models for Porous Media with Special Reference to Gas Flow, in Pore Structure and Properties of Materials, Proceedings of International Symposium RILEM/IUPAC, Prelim. Rpt. Part I, 1973, p. A-92.

25. S. Dushman, Scientific Foundations of Vacuum Technique, John Wiley and Sons, New York, 1955, p. 98.

26. Op. cit. Satterfield, pp. 35-41.

27. P. Mohazzabi, The Effect of Porous Barriers on the Molecular Compositions of Reactive Gas Mixtures. PhD thesis, University of California, February 1975. (LBL-3565)

28. "JANAF Thermochemical Data," Dow Chemical Co., Midland, Michigan, 1965.

29. P. Mohazzabi and A.W. Searcy, J. Chem. Phys. 65, 5037 (1977).

30. A.W. Searcy, The Kinetics of Evaporation and Condensation Reactions, in Chemical and Mechanical Behavior of Inorganic Materials, Wiley-Interscience, New York, 1970.

31. R.T. Grimley, Mass Spectrometry, in The Characterization of High Temperature Vapors, John Wiley and Sons, New York, 1967.

32. H. Yanagida and Y. Ono, J. Ceram. Assoc. Japan 76, 1 (1968).

Table 4. Transmission Probabilities for Permanent Gases, T = 295°K

Gas	W
Predicted: $(1/\tau)(4/3)(d/l)$	$1/\tau(13 \times 10^{-4})$
He	$(6.51 \pm .86) \times 10^{-4}$
Ar	$(6.86 \pm .63) \times 10^{-4}$
N_2	$(6.74 \pm .91) \times 10^{-4}$
CO_2	$(6.86 \pm .73) \times 10^{-4}$
O_2	$(6.80 \pm .63) \times 10^{-4}$
CH_4	$(5.43 \pm 1.26) \times 10^{-4}$
NH_3	$(6.01 \pm .60) \times 10^{-4}$
SO_2	$(6.59 \pm .65) \times 10^{-4}$

Table 5. Transmission Probabilities for Helium and High Temperature Vapors

Gas or vapor	Temperature °K	Number of measurements	Av. incident flux J_X mole/cm^{2}sec	Av. transmitted flux, J_L mole/cm^{2}sec	Av. transmission probability, W	J_S/J_K
He	295	4	-	-	$(6.51\pm.86)\times10^{-4}$	-
Zn	630	5	7.62×10^{-6}	6.16×10^{-9}	$(8.09\pm1.45)\times10^{-4}$	-
NaCl	1001	6	1.77×10^{-5}	3.00×10^{-8}	$(1.69\pm.23)\times10^{-3}$	1.6
NaF	1097	4	1.69×10^{-6}	6.61×10^{-9}	$(3.91\pm.43)\times10^{-3}$	5.0
LiF	1074	3	4.39×10^{-6}	3.49×10^{-8}	$(7.95\pm.68)\times10^{-3}$	11.2

Figure Captions

Fig. 13 Plot of residence time t vs E/RT.

Fig. 14 Pore sizes in the porous alumina, measured by a mercury porosimeter.

Fig. 15 Pore sizes in the porous alimina, measured by a mercury porosimeter.

Fig. 16 Micrograph of porous alimina.

Fig. 17 Micrograph of porous alimina.

Fig. 18 Apparatus for measuring transmission probabilities of permanent gases.

Fig. 19 Apparatus for measuring transmission probabilities of high temperature vapors.

Fig. 20 Plot of ln $I(Na^+)T$ vs 1/T for sodium chloride in a BN cell with an orifice and a porous barrier

Fig. 21 Plot of ln $I(Na^+)T$ vs 1/T for sodium chloride in a Al_2O_3 cell with an orifice and a porous barrier.

Fig. 22 Plot of ln $I(Li^+)T$ vs 1/T for lithium fluoride in a BN cell with an orifice and a porous barrier.

Fig. 23 Plot of ln $I(Li^+)T$ vs 1/T for lithium fluoride in a Al_2O_3 cell with an orifice and a porous barrier.

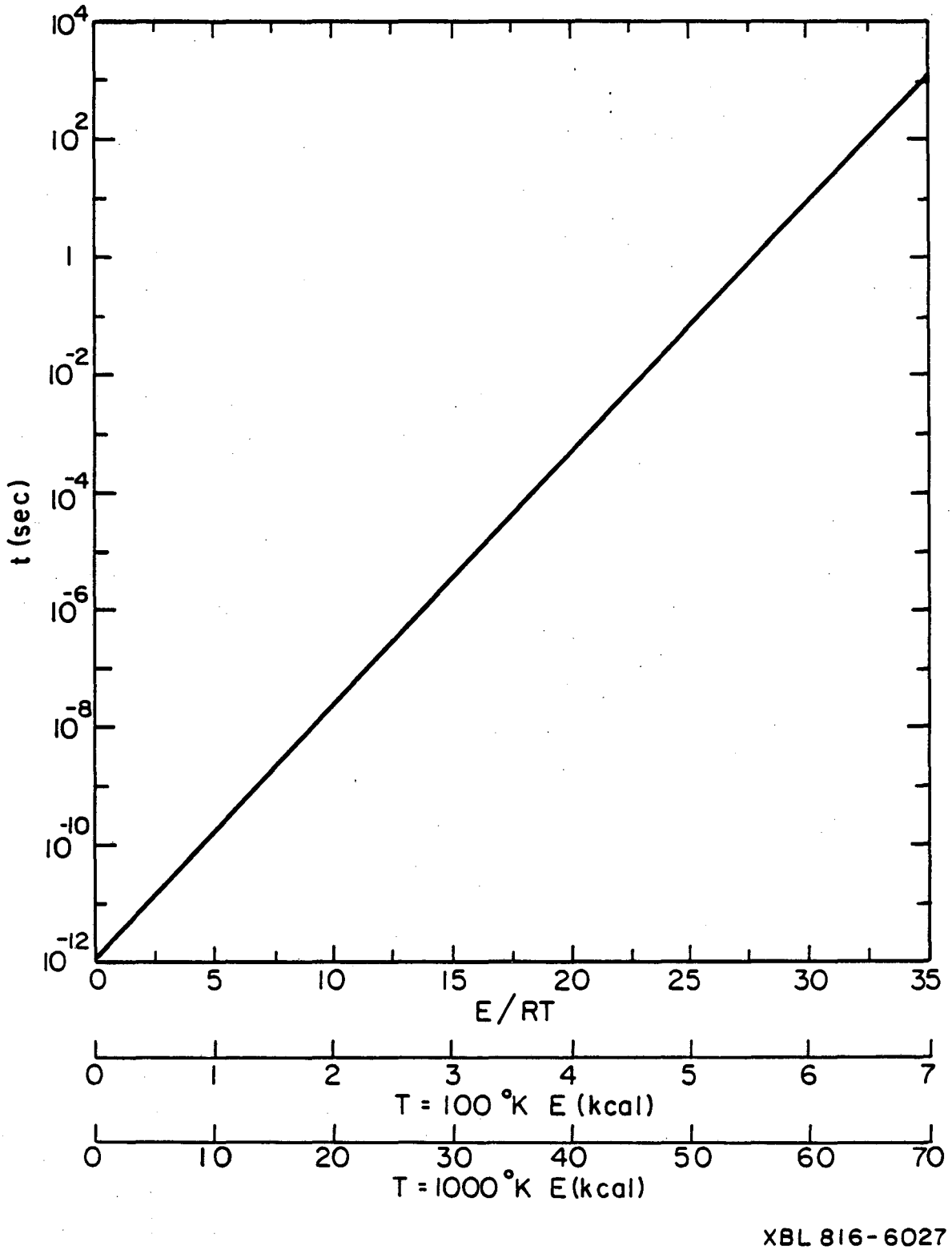
10^4
10^2
1
10^{-2}
10^{-4}
10^{-6}
10^{-8}
10^{-10}
10^{-12}
t (sec)
0 5 10 15 20 25 30 35
E / RT
0 1 2 3 4 5 6 7
T = 100 °K E (kcal)
0 10 20 30 40 50 60 70
T = 1000 °K E (kcal)
XBL 816-6027

Figure 13

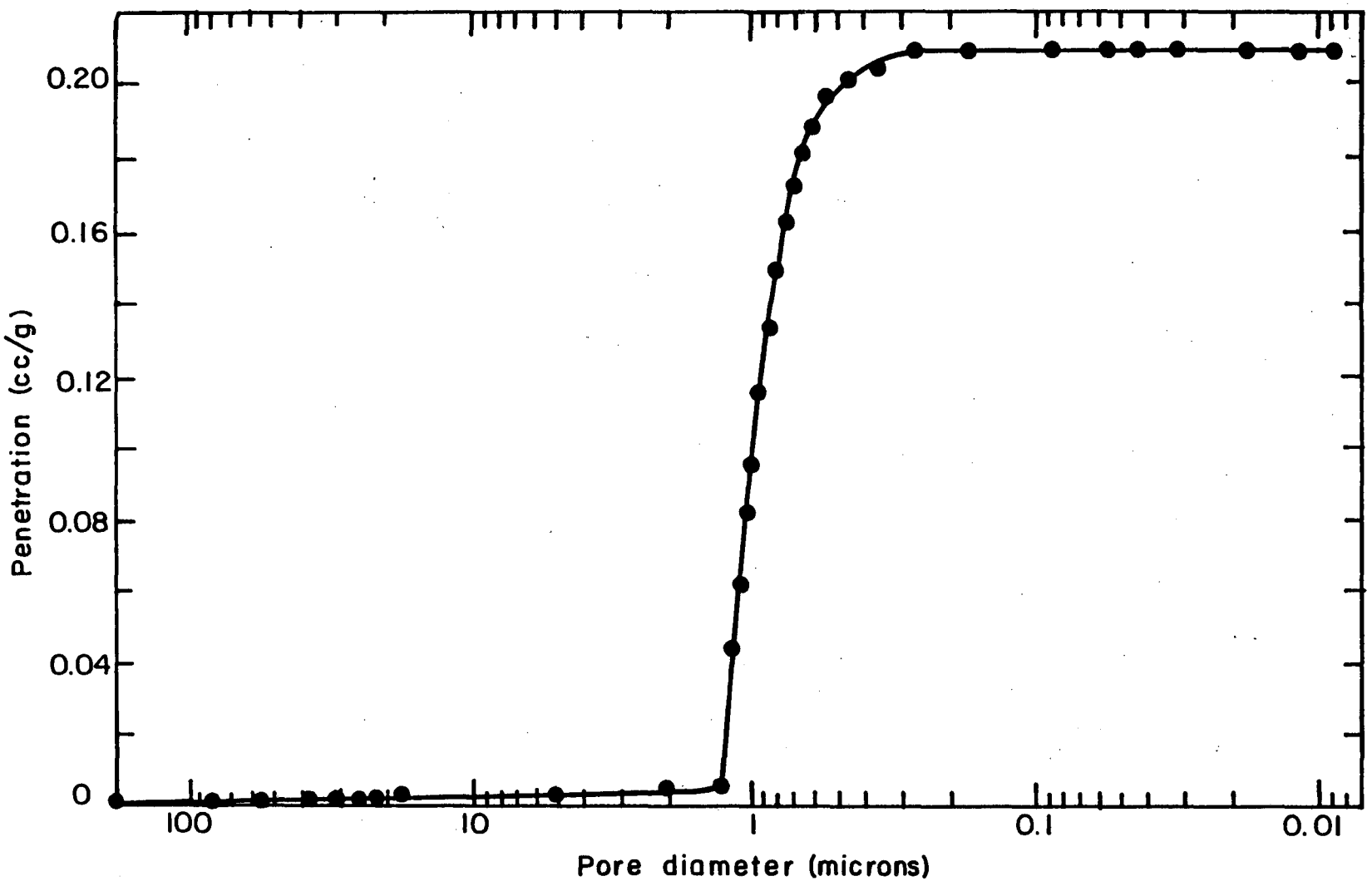

XBL 817-6109

Figure 14

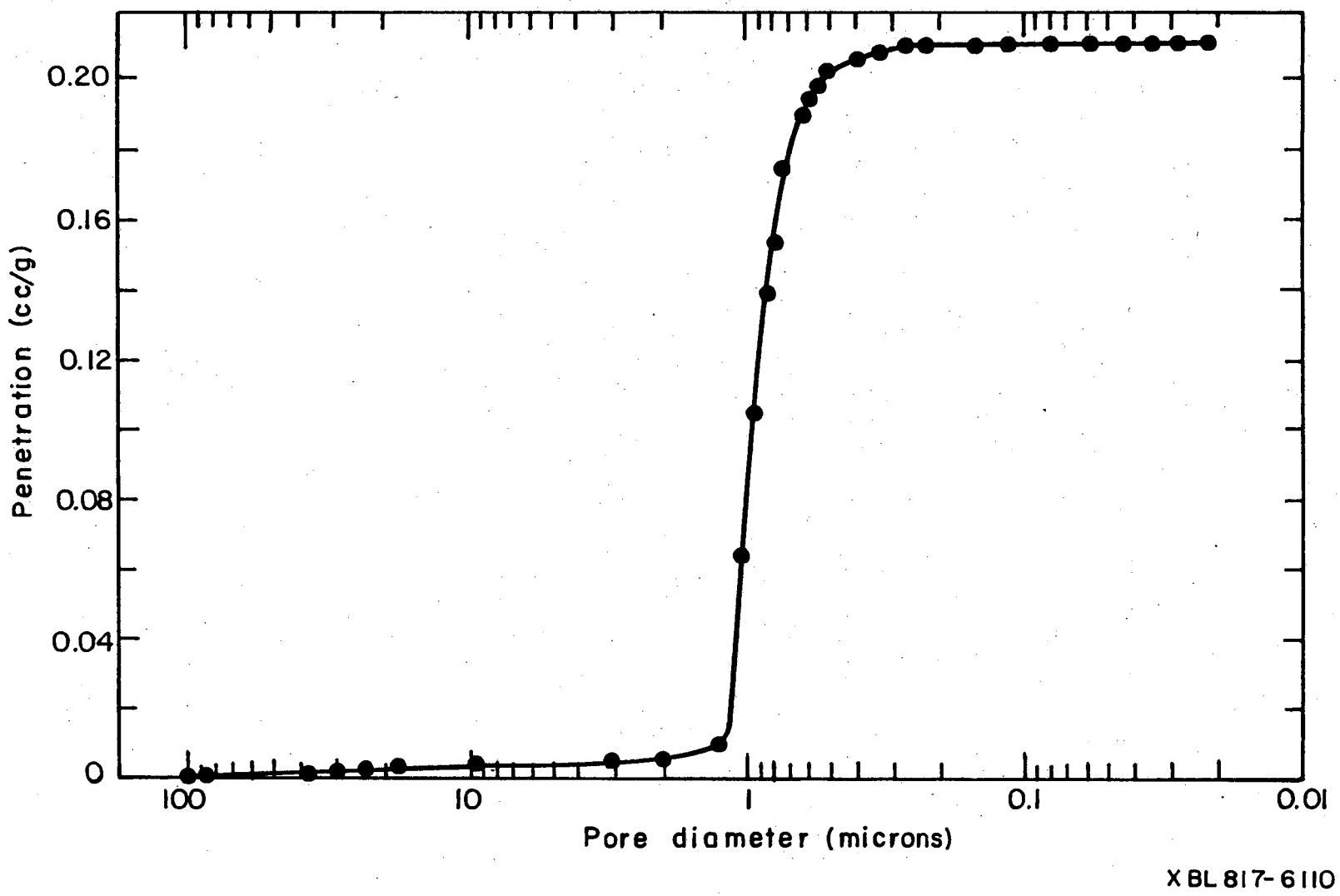
0.20
0.16
0.12
0.08
0.04
0
Penetration (cc/g)
100
10
1
0.1
0.01
Pore diameter (microns)
XBL 817-6110

Figure 15

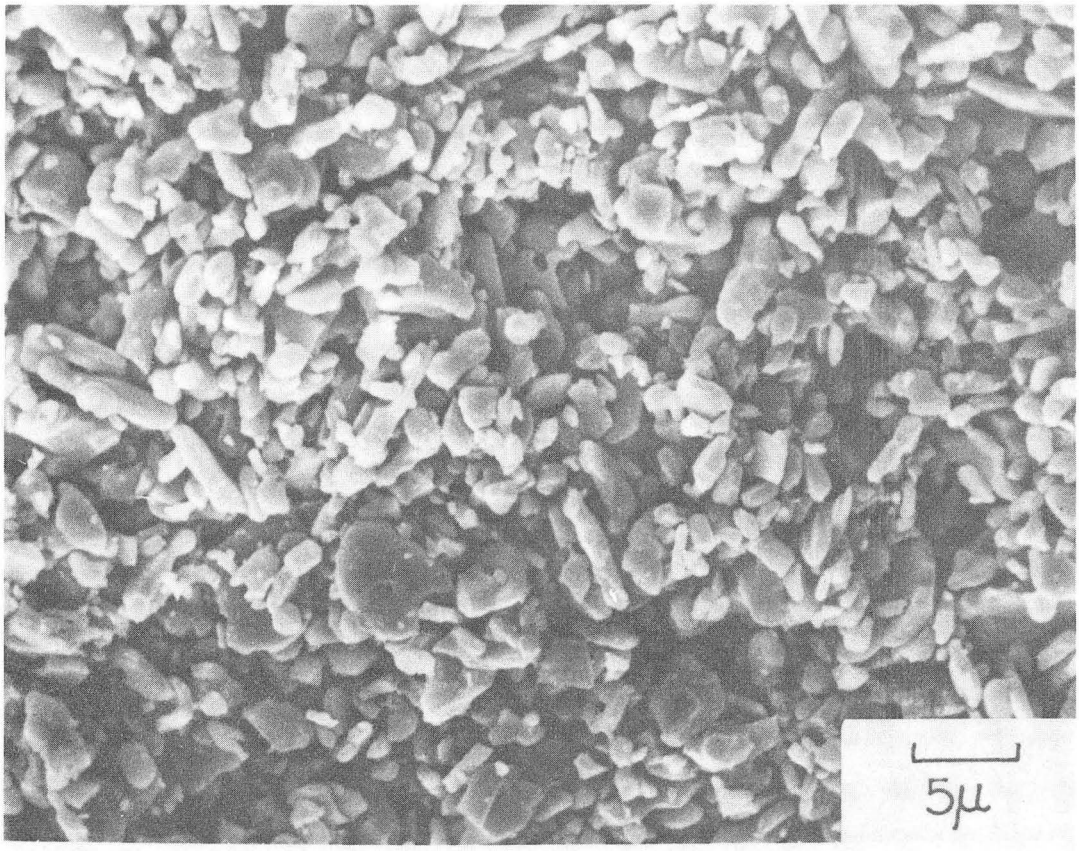

XBB 813-2924

Figure 16

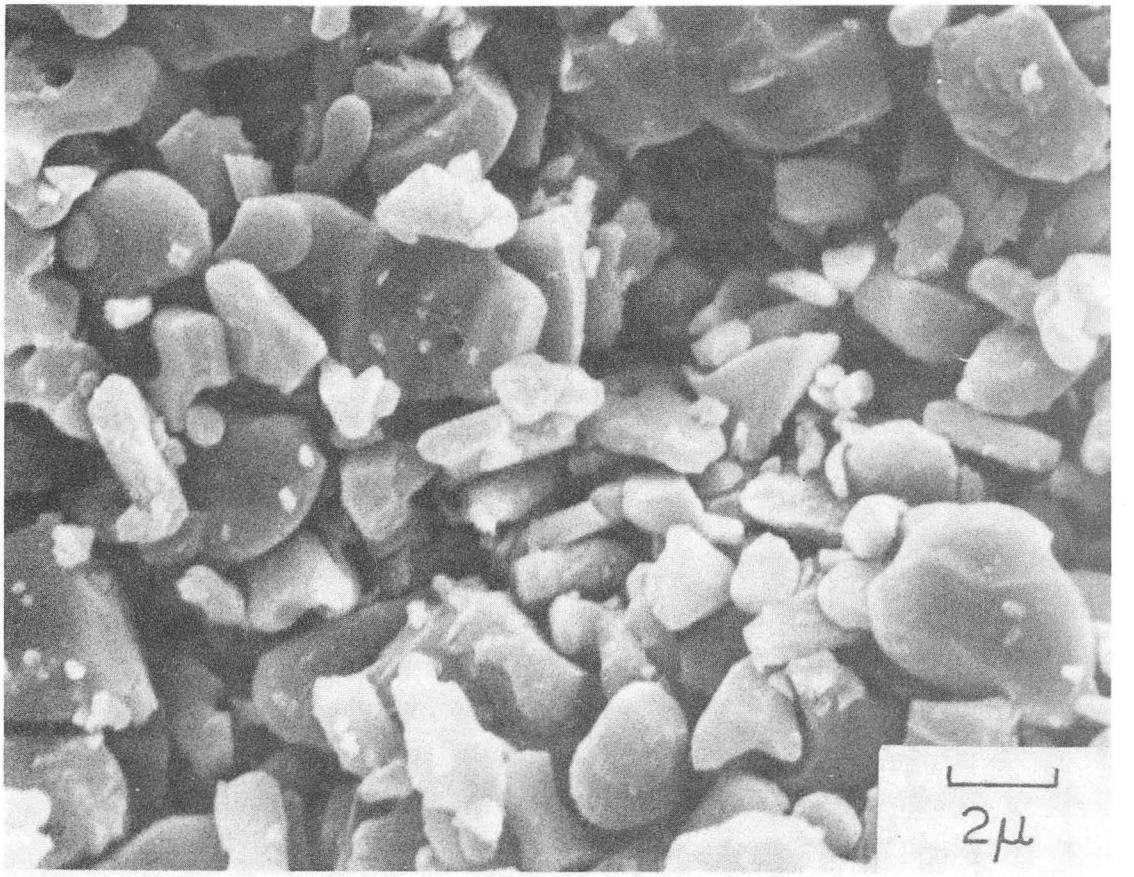

XBB 813-2925

Figure 17

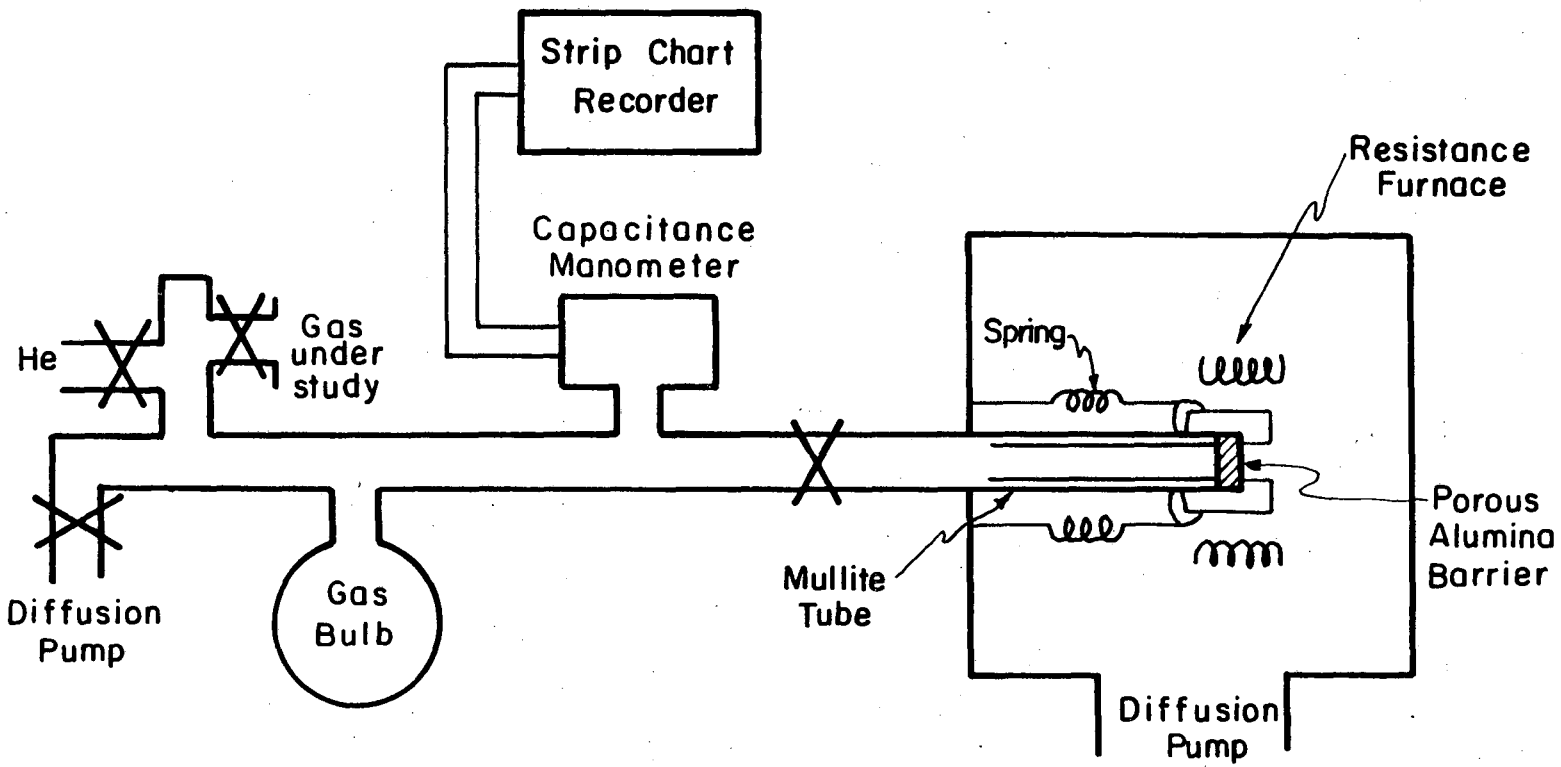

XBL816-6029

Figure 18

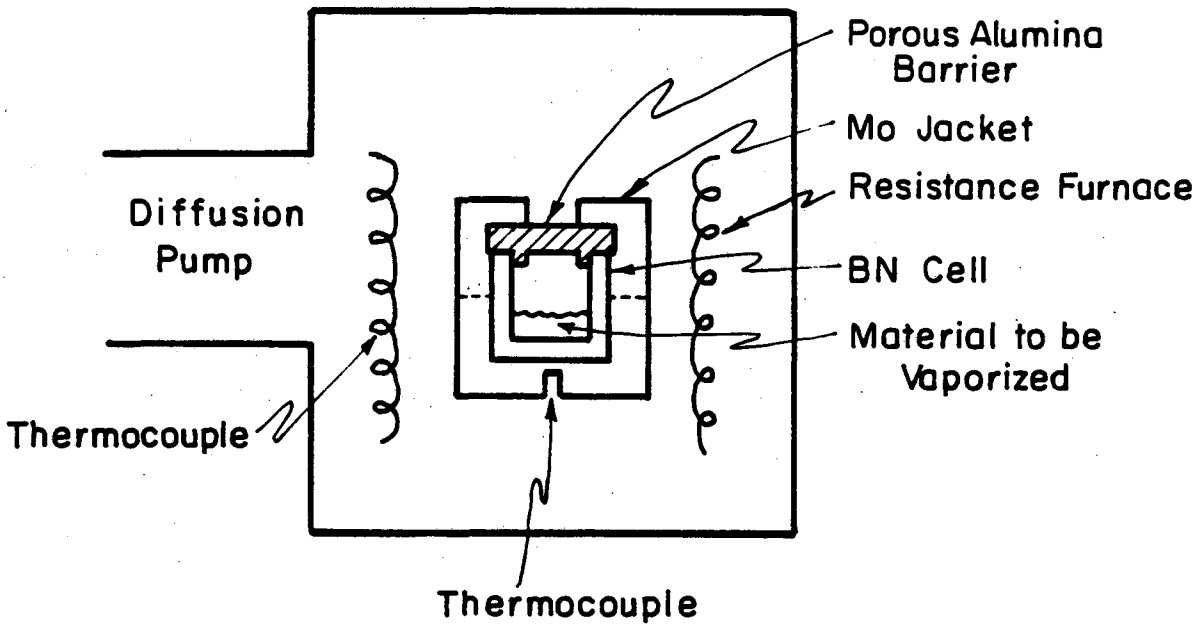

XBL 816-6030

Figure 19

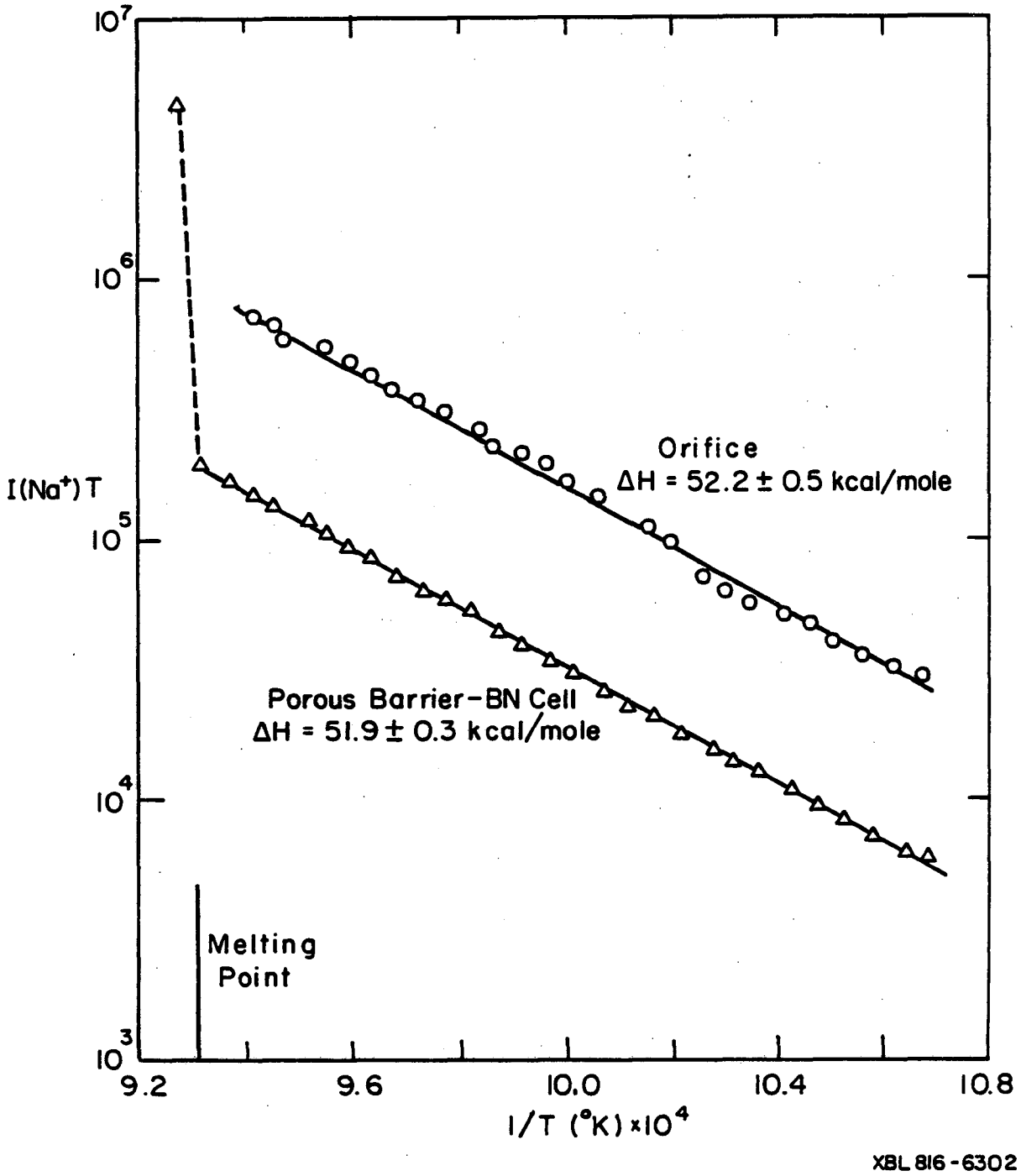
10^7
10^6
10^5
10^4
10^3
I(Na⁺) T
Orifice
ΔH = 52.2 ± 0.5 kcal/mole
Porous Barrier-BN Cell
ΔH = 51.9 ± 0.3 kcal/mole
Melting
Point
9.2
9.6
10.0
10.4
10.8
1/T (°K) ×10⁴
XBL 816-6302

Figure 20

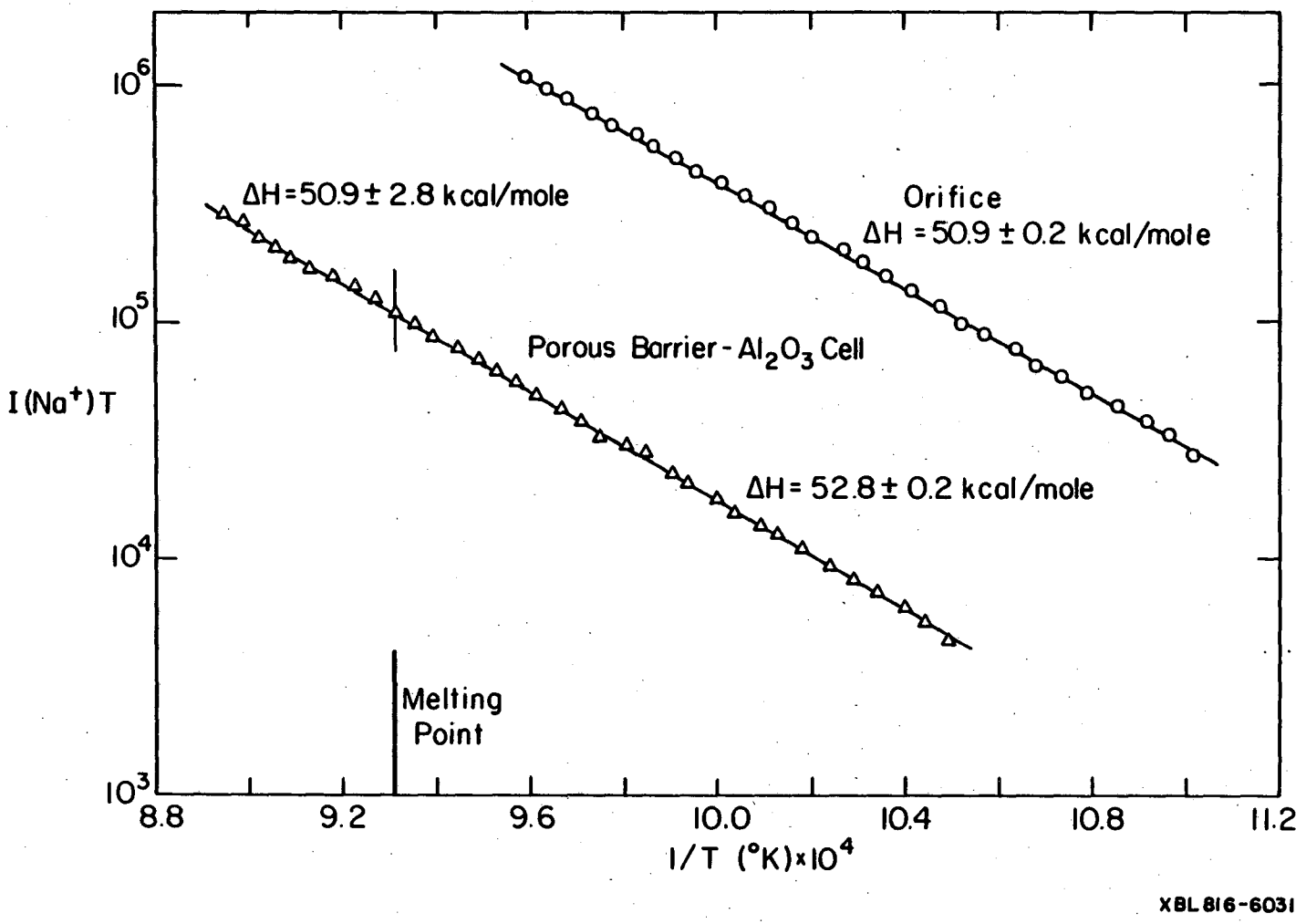
ΔH=50.9 ± 2.8 kcal/mole
Orifice
ΔH = 50.9 ± 0.2 kcal/mole
Porous Barrier - Al_2O_3 Cell
ΔH= 52.8 ± 0.2 kcal/mole
Melting Point
$I(Na^+)T$
10^6
10^5
10^4
10^3
8.8
9.2
9.6
10.0
10.4
10.8
11.2
$1/T\ (°K) \times 10^4$
XBL 816-6031

Figure 21

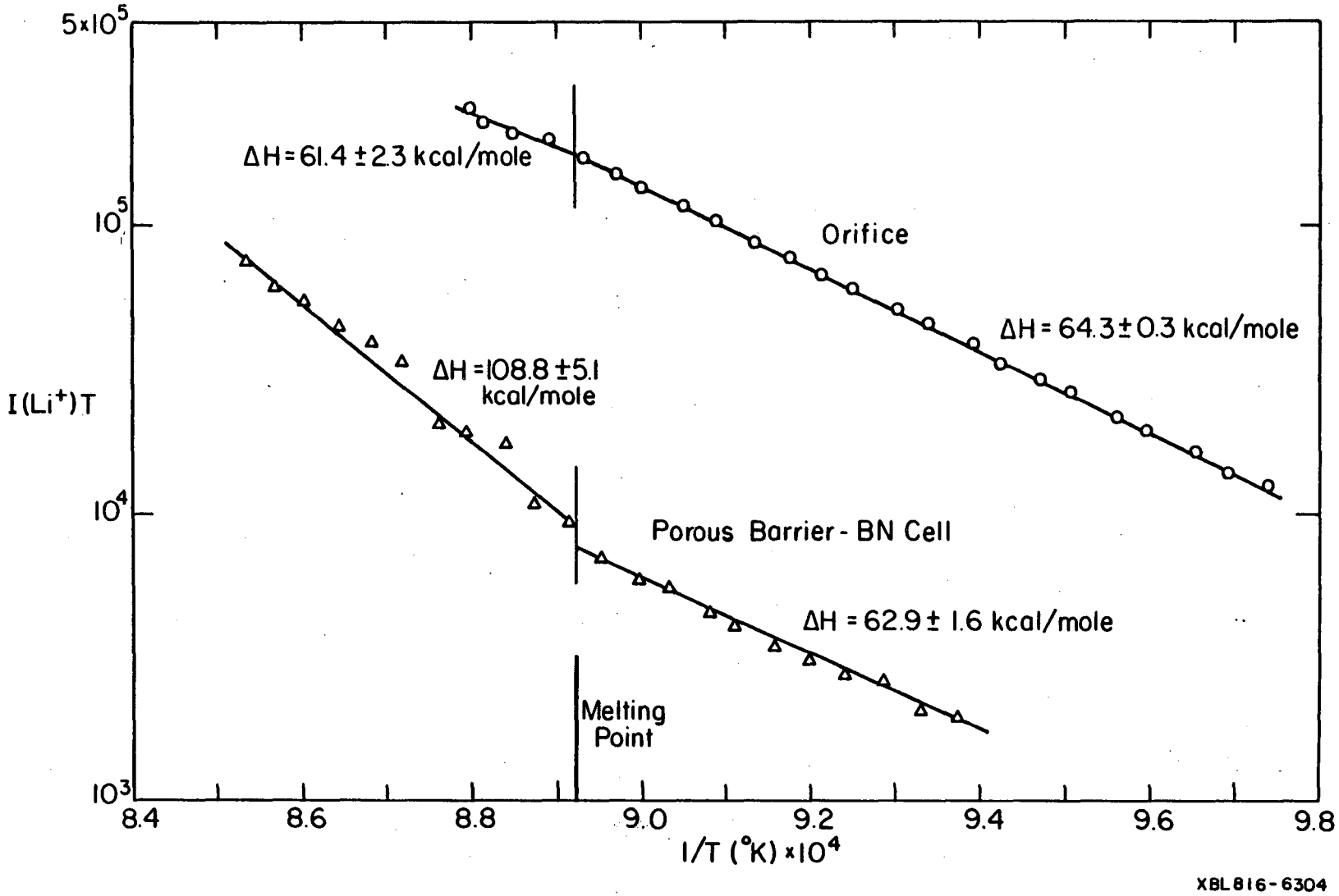
5×10^5
10^5
10^4
10^3
I(Li+)T
ΔH=61.4 ±2.3 kcal/mole
Orifice
ΔH = 64.3±0.3 kcal/mole
ΔH =108.8 ±5.1 kcal/mole
Porous Barrier - BN Cell
ΔH = 62.9 ± 1.6 kcal/mole
Melting Point
8.4
8.6
8.8
9.0
9.2
9.4
9.6
9.8
1/T (°K) ×10^4
XBL816-6304

Figure 22

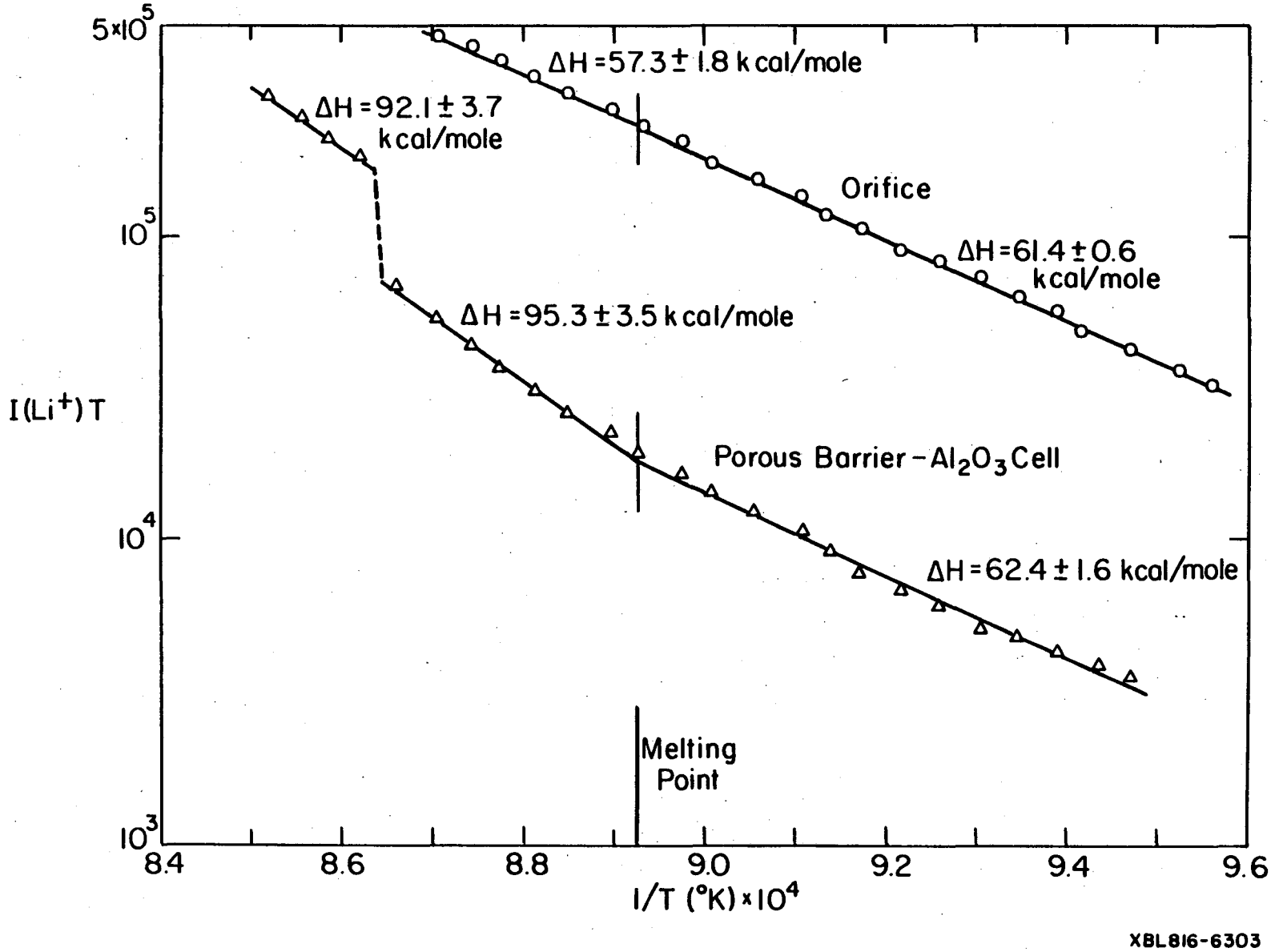

XBL816-6303

Figure 23

ACKNOWLEDGMENT

I extend my deepest gratitude to Professor Alan W. Searcy for his guidance and encouragement throughout this study. Working under Professor Searcy has been a period of both professional and personal growth.

I am also grateful to Dr. David Meschi for his frequent help and advice, particularly with the mathematics of Part I. I would like to thank Professor James W. Evans, whose fine courses inspired many parts of this work.

It has been an enjoyable and enriching experience working with my fellow students--T. Dai, J. Farnsworth, L. Feldman, P. Flaitz, D. Goodman, E. Opila, R. Shukla, T. Reis, and S. Roche.

The LBL technicians--particularly G. Baum, H. Brendl, K. Gaugler, M. Kujala, J. Severns, W. Wong, B. Wilke, and W. Lawrence--deserve a special thanks. These men went well beyond their duties by being especially helpful. I am also grateful to my special friend--Mamie Brown--for her support and encouragement.

Finally, I would like to thank my parents and friends outside the laboratory for their support.

This work was funded by the Division of Materials Sciences, Office of Basic Energy Sciences, U.S. Department of Energy under Contract W-7405-ENG-48.

This report was done with support from the Department of Energy. Any conclusions or opinions expressed in this report represent solely those of the author(s) and not necessarily those of The Regents of the University of California, the Lawrence Berkeley Laboratory or the Department of Energy.

Reference to a company or product name does not imply approval or recommendation of the product by the University of California or the U.S. Department of Energy to the exclusion of others that may be suitable.

TECHNICAL INFORMATION DEPARTMENT
LAWRENCE BERKELEY LABORATORY
UNIVERSITY OF CALIFORNIA
BERKELEY, CALIFORNIA 94720